



Influence of the number of cells on the stress distribution in a running PEM fuel cell stack

Maher A.R. Sadiq Al-Baghdadi

Fuel Cell Research Center, International Energy and Environment Foundation, Najaf, P.O.Box 39, Iraq.

Received 4 Oct. 2017; Received in revised form 12 Nov. 2017; Accepted 1 Dec. 2017; Available online 1 Mar. 2018

Abstract

Mechanical degradation is often studied in single-cell proton exchange membrane (PEM) fuel cell stack models in assembly process. This however, can increase substantially when moving from assembly process to operation conditions; and also from single-cell to multiple cells. In this study, PEM fuel cell stacks consisting of 1, 3, and 5 cells with an active area of 25 cm² per cell have been simulated in operation mode. Three dimensional non-isothermal solid mechanics-CFD model of a PEM fuel cell stack, integrating the real full scale geometry of all components have been used to study the influence of the number of cells on the stress distribution in a running PEM fuel cell stack. Simulation of a running multi cells stack was successful and has not been previously seen in literatures work. The results showed that the center of the electrode tends to un-displacement. This un-displacement area increases by increasing the clamping torque. The deformations in the stack components during operation were about ten times higher than during assembly process. During assembly process, the increasing in the number of cells increases the total displacement distribution. These status were different during operation, the increasing in the number of cells enhances the uniformity of the total displacement. Increasing the number of cells enhances the uniformity of the mechanical state. The better contact pressure homogeneity was obtained with the greater number of cells and leads to the lower contact resistance. In general, the results showed lower stresses values with lower distributions and more homogeneous and uniformity in the stack that consisting of multi cells.

Copyright © 2018 International Energy and Environment Foundation - All rights reserved.

Keywords: 3D PEM fuel cell stack; CFD; Stack modeling; Mechanical analysis; Thermal stress.

1. Introduction

The need for improved lifetime of PEM fuel cell stacks necessitates that the failure mechanisms be clearly understood and life prediction models be developed, so that new designs can be introduced to improve long-term performance. Increasing of the durability is a significant challenge for the development of fuel cell technology [1].

The Membrane-Electrode-Assembly (MEA) is the core component of PEM fuel cell stack and consists of membrane with the catalyst layers (CL) attached to each side. The fuel cell MEA durability plays a vital role in the overall lifetime achieved by a stack in field applications. Mechanical stresses which limit MEA durability have two origins [1, 2]. Firstly, this is the stresses arising during fuel cell assembly (bolt assembling). The bolts provide the tightness and the electrical conductivity between the contact elements. Secondly, additional mechanical stresses occur during fuel cell running because PEM fuel cell stack

components have different thermal expansion and swelling coefficients. Thermal and humidity gradients in the fuel cell stack produce dilatations obstructed by tightening of the screw-bolts. Compressive stress increasing with the hygro-thermal loading can exceed the yield strength which causes the plastic deformation. The mechanical behaviour of the membrane depends strongly on hydration and temperature [1, 2]. Variations in temperature and humidity during operation cause stresses and strains (mechanical loading) in the membrane as well as in all components and are considered to be the mechanical failure driving force in fuel cell applications [1-3]. Investigating the mechanical response of the PEM fuel cell stack during operation (subjected to change in humidity and temperature) requires studying and modelling of the stress-strain behaviour of all fuel cell stack components in operation phase [4, 5].

Wen et al. [6] was used pressure sensitive film for studying clamping pressure on a single cell and 10-cell stack in order to find the optimum bolt configuration and clamping pressure. The results showed that decreases in porosity of the GDL did not appear to have a significant effect in the 10-cell stack. They also showed that increasing clamping pressure improved pressure distribution, however; maximum power did not increase monotonically. It appears that cell to cell variations mean local pressure distributions have an important influence.

Carral and Mele [7] developed a 3D finite element model to investigate the influence of the assembly phase of PEM fuel cell stacks on the mechanical state of the active layer (MEA). The results showed that better uniformity of the MEA compression is obtained with the greatest number of cells, and at the center of the stack. However, they not integrate stamped metallic bipolar plates due to the difficulty of the simulation.

Bates et al. [8] simulated a PEM fuel cell stack at various clamping pressures during assembly, resulting in detailed 3D plots of stress and deformation distribution in all materials of the stack. This type of simulation can be very revealing as to the effectiveness of a stack assembly. However, all components in this model are modeled as 3D objects and keep their general form, and all features have been removed from the materials except for gas channels in the bi-polar plates. They explained that the full stack analysis requires significant computing power.

Cruz et al. [9] performed a numerical simulation in order to obtain the mechanical stress distribution during assembly process for two of the most pressure sensitive components of the stack: the membrane, and the graphite plates. The stress distribution of the above mentioned components was numerically simulated by finite element analysis and the stress magnitude for the membrane was confirmed using pressure films. The analysis showed that gas inlet and outlet zones, as well as areas of the membrane in contact with rigid components require special considerations during design to avoid stress concentration. The use of materials to dissipate the load stress and protect sensitive materials can be an alternative to maintain the integrity of the fuel cell stack and prologue its lifetime.

Charon et al. [10] suggested a numerical method towards stress calculation in a PEM fuel cell stack. A finite element model submitted to operational static load is developed for pure mechanical analysis of a stack. They applied the homogenisation technique by replacing cell parts with composite finite elements or homogenised representative elementary volumes. Then a fuel cell stack model is built and finally computed using homogenised properties. The distribution of stresses computed at stack level was applied as boundary conditions on detailed models for only a selected sensitive area to analyse local phenomena. However, their method gives good results for the calculation of stresses due to the assembly process. But as soon as the fuel cell is in operation, other physical phenomena must be considered, especially heat exchanges and the swelling of the membrane due to hydration. They concluded that finding the local stress of a stack in operation is difficult. It requires multi-physics studies, including both solid and fluid mechanics and also electrochemistry. So their work is a step towards stress calculation in a stack in operation.

Chien et al. [11] established three-dimensional finite element model of a bolted PEM fuel cell stack using the commercial software SolidWorks 2012. Then, the model was analysed though commercial software ANSYS 15.0 while the model was subjected to different bolt pre-loadings and thermal loading. Finally, the effects of variations of bolt pre-loading on the contacting pressure, compression ratio, contact resistance, porosity and flow channel intrusion rate of GDL in a PEM fuel cell were investigated and discussed. However, in their model an internal heat resource was assumed and applied to the membrane, catalyst layers, and GDLs to simulate the generation of heat by the chemical reactions. The obtained temperature distribution was used to determine the deformation and stress of the PEM fuel cell subjected to bolt pre-loadings. In addition, the swelling of the membrane due to hydration was not considered and modelled. The hydrations have a bigger effect than temperature in developing mechanical stresses in the

membrane. These stresses will be more critical when non-uniformity as a form of hydration profile across the membrane [4, 5].

In summary, this state of the art shows that the existing models are completely based on mechanical analysis of a stack not in the case of the operating (i.e. during assembly process only). In order to acquire a complete understanding of the damage mechanisms in the membranes and the rest of the stack components, mechanical response under hydration and thermal loads should be studied under realistic stack operating conditions. In this study, PEM fuel cell stacks consisting of 1, 3, and 5 cells with an active area of 25 cm² per cell have been simulated in operation mode. Three dimensional non-isothermal solid mechanics-CFD model of a PEM fuel cell stack, integrating the real full scale geometry of all components will be used to study the influence of the number of cells on the stress distribution in a running PEM fuel cell stack.

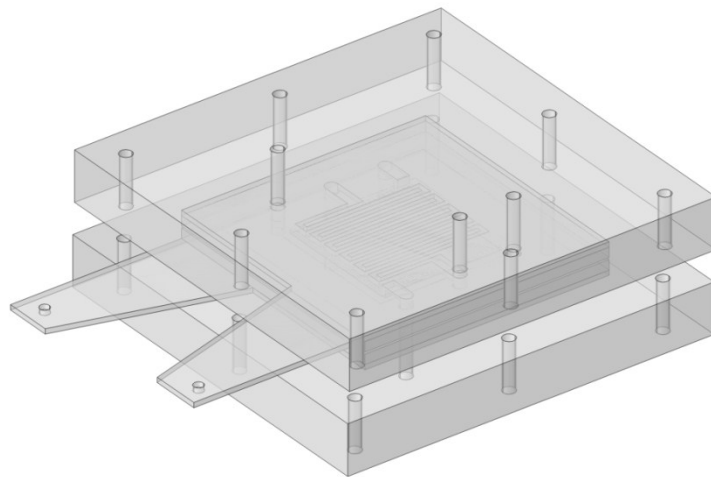
2. PEM fuel cell stack model

The difficult experimental environment of fuel cell systems has stimulated efforts to develop models that could simulate and predict multi-dimensional coupled transport of reactants, heat and charged species, in addition to mechanical analysis using computational fluid dynamic methods (CFD) and Finite Element Methods (FEM).

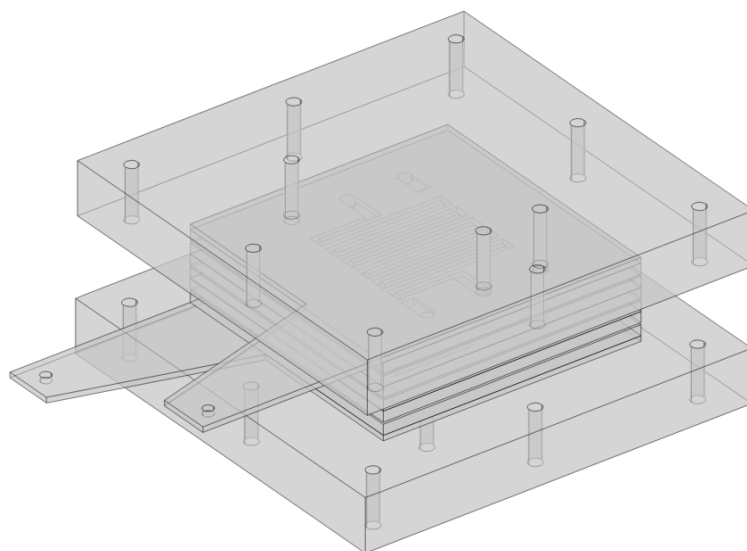
CFD and FEM are the sciences of predicting fluid flow, heat transfer, mass transfer, phase change, chemical reaction, mechanical movement, stress or deformation of related solid structures, and related phenomena by solving the mathematical equations that govern these processes using a numerical algorithm on a computer. We typically use CFD to simulate and analyse fluids and flow and FEM to simulate and analyse various stresses and forces on solids. The results of CFD and FEM analyses are relevant in: conceptual studies of new designs, detailed product development, troubleshooting, and redesign. CFD and FEM analysis complements testing and experimentation, by reduces the total effort required in the experiment design and data acquisition. CFD and FEM complements physical modelling and other experimental techniques by providing a detailed look into our engineering problems, including complex physical processes such as turbulence, chemical reactions, heat and mass transfer, multiphase flows, and mechanical behaviours. Simulations can readily be done of physical phenomena that are difficult to measure, for example, full scale situations, environmental effects and hazards. In many cases, we can build and analyse virtual models at a fraction of the time and cost of physical modelling. This allows us to investigate more design options and "what if" scenarios than ever before. Moreover, chemical reaction and flow modelling provides insights into our fluid flow problems that would be too costly or simply prohibitive by experimental techniques alone. The added insight and understanding gained from flow modelling gives us confidence in our design proposals, avoiding the added costs of over-sizing and over-specification, while reducing risk.

CFD and FEM modelling are great tools for the design and analyses of fuel cell stack. The strength of these numerical approaches are in providing detailed insight into the various transport mechanisms and their interaction, and in the possibility of performing parameters sensitivity analyses. These models allow engineers and designers to predict the performance of the fuel cell given design parameters, material properties and operating conditions.

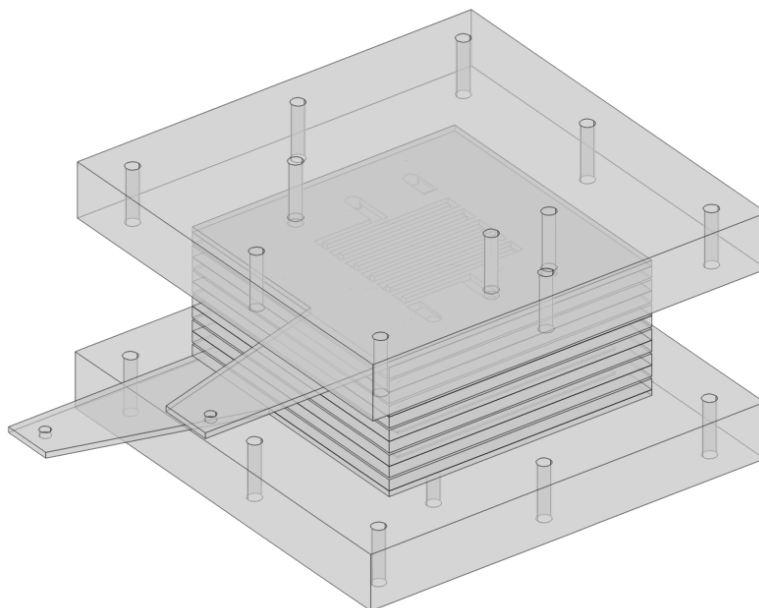
Three dimensional non-isothermal solid mechanics-CFD model of a PEM fuel cell stack integrating the real full scale geometry of all components have been developed, validated, and discussed in detail by the current author in his previous paper [12] and it was used in this work to study the influence of the number of cells on the stress distribution in a running PEM fuel cell stack. In brief, the model is based on full three-dimensional, non-isothermal computational fluid dynamics (CFD) detailed model of a PEM fuel cell stack and considers multi-phase, multi-component flow inside the gas flow channels and the porous media of a PEM fuel cell stack and coupled with a solid mechanics model to simulate the stress distribution inside the stack, which are occurring during fuel cell assembly (bolt assembling), and membrane swelling and cell materials expansion during fuel cell running due to the changes of temperature and relative humidity. PEM fuel cell stacks with clamping plate and rod assembly for a number of cells equal to 1, 3 and 5 are shown in Figure 1. The stack model simulated includes the following components; two end-plates, two current plates, two bi-polar plates, two GDLs, two gaskets, and, an MEA (membrane plus two CLs) as shown in Figure 2. Both cathode and anode have straight gas flow channels in square cross section area of 1mm. The upper face of the cathode bi-polar plate has a serpentine water flow channel in square cross section area of 2 mm. Material properties and dimensions of each component are shown in Table 1.



(a) PEM fuel cell stack consisting of single cell.



(b) PEM fuel cell stack consisting of three cells.



(c) PEM fuel cell stack consisting of five cells.

Figure 1. Three-dimensional computational domain for the PEM fuel cell stacks.

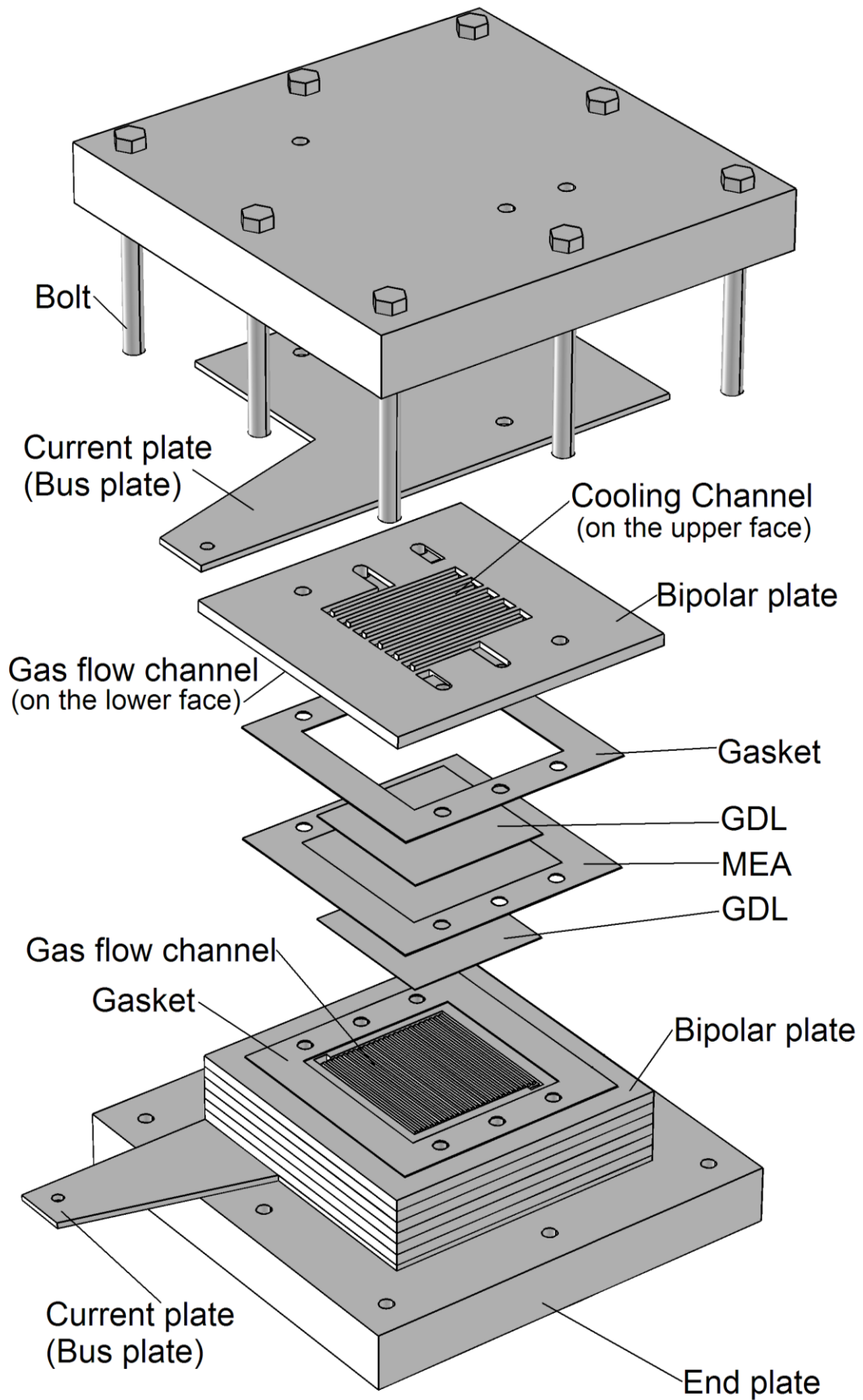


Figure 2. Description of the different stack components in computational domain.

Table 1. Properties and dimensions of the stack components.

Property	MEA	GDL	Bipolar plate	Current collector	Gasket	End plate
Material	Nafion [®]	Carbon paper	Carbon graphite	C15720 copper	Silicon [®]	Stainless steel
Young's modulus [GPa]	Table 2	10	10	110	0.54	209
Density [kg/m ³]	2000	400	1800	8700	2330	7800
Poisson's ratio	0.25	0.25	0.25	0.35	0.30	0.25
Expansion coeff. [K ⁻¹]	123e ⁻⁶	-0.8e ⁻⁶	5e ⁻⁶	17e ⁻⁶	62e ⁻⁶	12e ⁻⁶
Conductivity [W m ⁻¹ K ⁻¹]	0.455	17.122	95	385	0.517	44.5
Specific heat [J kg ⁻¹ K ⁻¹]	1050	500	750	385	932	460
Dimensions [mm]	80 x 80	50 x 50	100 x 100	100 x 100	80 x 80	150 x 150
Thickness [mm]	0.24	0.26	4	2	0.26	20

Table 2. Young's modulus at various temperatures and humidities of Nafion[®].

Young's modulus [MPa]	Relative humidity [%]			
	30	50	70	90
T=25 C	197	192	132	121
T=45 C	161	137	103	70
T=65 C	148	117	92	63
T=85 C	121	85	59	46

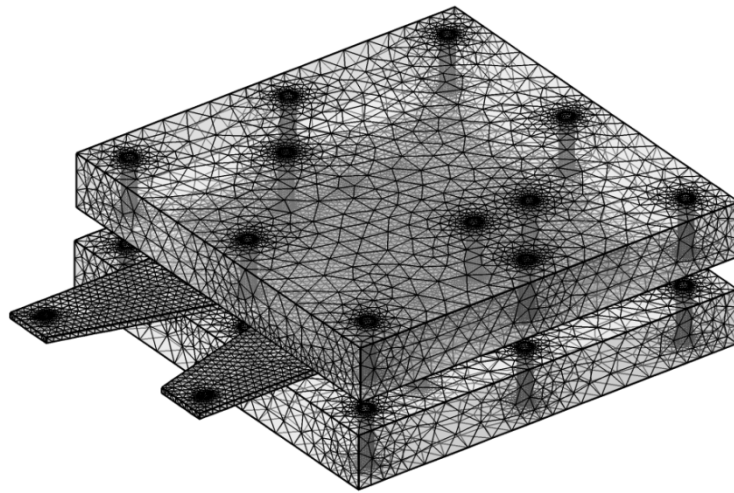
2.3. Modelling parameters

Choosing the right modelling parameters is important in establishing the base case validation of the model against experimental results. Since the fuel cell stack model that is presented in this study accounts for all basic transport phenomena simply by virtue of its three-dimensionality, a proper choice of the modelling parameters will make it possible to obtain good agreement with experimental results obtained from a real fuel cell stack. It is important to note that because this model accounts for all major transport processes and the modelling domain comprises all the elements of a complete fuel cell stack, no parameters needed to be adjusted in order to obtain physical results.

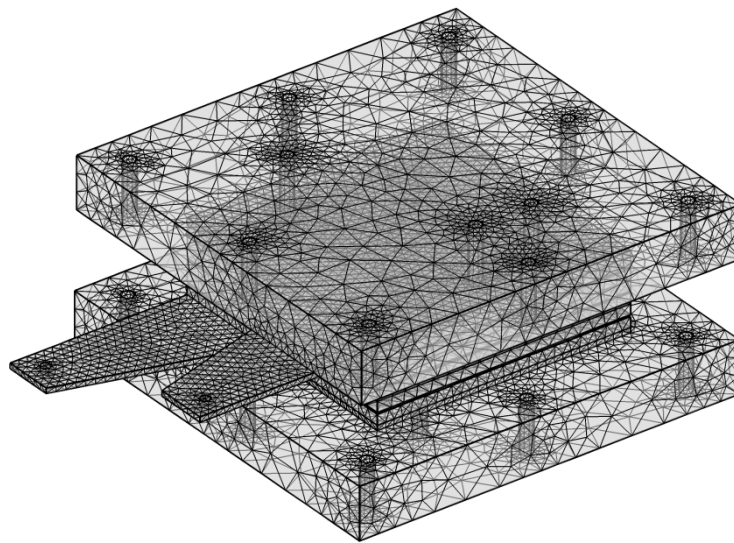
The assembly conditions are set to reference temperature 20 C, and relative humidity 30%, where the thermal strain of the all stack components and the swelling strain of the membrane are equals to zero. The clamping forces of the nut and bolt are applied on a specific area of the end plates in the assembly procedure. The assembly was clamped together with eight bolts. The model presented in this work takes more factors into consideration during assembly such as thread pitch, bolt diameter, and friction factors. A friction factor of 0.2 is used with a torque of 5 N.m which is equivalent to a 5000 N axial load per bolt. The cell operates at a nominal current density of 1.2 A/cm². The selection of relatively high current density is due to illustrate the phase change effects, membrane swelling and thermal stresses which are more visible in the stack in the high loading conditions. Values of the operating conditions and electrochemical transport parameters are listed in Table 3. The governing equations were discretized using a finite-volume method and solved using a multi-physics computational fluid dynamic (CFD) code. Stringent numerical tests were performed to ensure that the solutions were independent of the grid size (Figure 3). The coupled set of equations was solved iteratively, and the solution was considered to be convergent when the relative error was less than 1.0×10^{-6} in each field between two consecutive iterations.

Table 3. Operating conditions and electrochemical transport parameters [12].

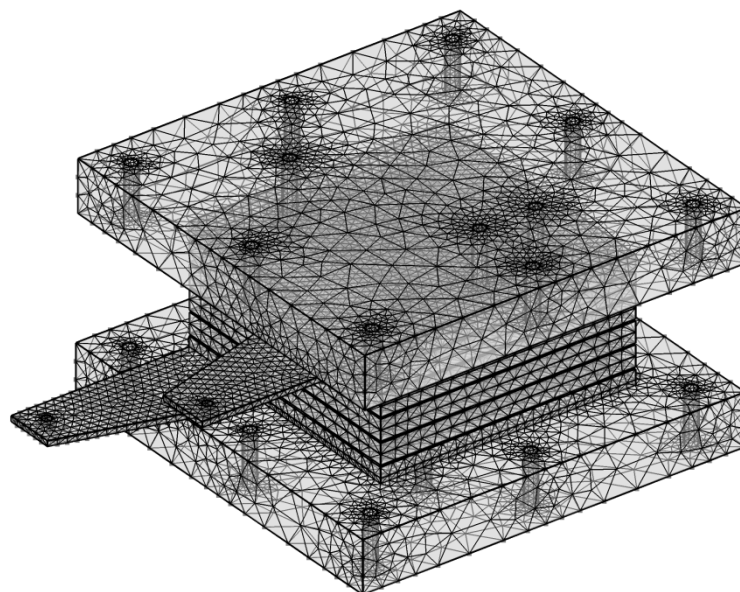
Parameter	Symbol	Value
Air pressure (Cathode pressure) [atm]	P_c	3
Fuel pressure (Anode pressure) [atm]	P_a	3
Air stoichiometric flow ratio	ξ_c	2
Fuel stoichiometric flow ratio	ξ_a	2
Relative humidity of inlet air [%]	\mathfrak{R}_c	100
Relative humidity of inlet fuel [%]	\mathfrak{R}_a	100
Ambient temperature [K]	T_{amb}	298.15
Air inlet temperature [K]	T_{cell}	353.15
Fuel inlet temperature [K]	T_{cell}	353.15
Inlet Oxygen/Nitrogen ratio	ψ	0.79/0.21
Hydrogen reference mole fraction	$x_{H_2}^{ref}$	0.84639
Oxygen reference mole fraction	$x_{O_2}^{ref}$	0.17774
Electrode initial porosity	ε	0.4
Electrode electronic conductivity	λ_e	100 S/m
Membrane ionic conductivity (Nafion®117)	λ_m	17.1223 S/m
Transfer coefficient, anode side	α_a	0.5
Transfer coefficient, cathode side	α_c	1
Cathode reference exchange current density	$i_{o,c}^{ref}$	$1.8081e^{-3}$ A/m ²
Anode reference exchange current density	$i_{o,a}^{ref}$	2465.598 A/m ²
Electrode thermal conductivity	k_{eff}	1.3 W/m.K
Membrane thermal conductivity	k_{mem}	0.455 W/m.K
Electrode hydraulic permeability	k_p	$1.76e^{-11}$ m ²
Entropy change of cathode side reaction	ΔS	-326.36 J/mol.K
Heat transfer coef. between solid and gas phase	β	4e6 W/m ³
Protonic diffusion coefficient	D_{H^+}	$4.5e^{-9}$ m ² /s
Fixed-charge concentration	c_f	1200 mol/m ³
Fixed-site charge	z_f	-1
Electro-osmotic drag coefficient	n_d	2.5
Droplet diameter	D_{drop}	$1e^{-8}$ m
Condensation constant	C	$1e^{-5}$
Scaling parameter for evaporation	ϖ	0.01



(a) PEM fuel cell stack consisting of single cell.



(b) PEM fuel cell stack consisting of three cells.



(c) PEM fuel cell stack consisting of five cells.

Figure 3. Computational mesh of a PEM fuel cell stack.

3. Results and discussion

The use of the CFD allows the study of the physical phenomenon within a fuel cell stack such as heat and energy transport without the need to build a structure, eliminating the manufacture and machining costs. The 3D model enables the prediction of the distribution and visualization of various parameters influencing the stack behaviour .

Figure 4 represents the temperature within the different components of the single, three, and five stacks respectively. It is seen that the highest temperature is located close to the cathode catalyst layer, implying that major heat generation takes place in this region. The temperature over the bipolar plates is quite uniform with peaks coming from the heat production within the MEA (mainly within cathode side reaction layers). Overall, the temperature within the centre of the stacks is 8°C higher than the mean operating temperature of 80°C. Along with the figure, the temperature distribution decreases from inside to the outside walls due to heat flow to the ambient temperature. It is seen that the boundary temperature is lowest (close to 78°C) at the bipolar plates, current collectors, and end plates boundaries due to the large temperature difference (heat loss towards the surroundings). The results also showed that in large number of cells in the stacks, heat conduction is insufficient to remove the excess of heat generation; therefore, the temperature difference will be reduced since much more heat is produced internally.

The PEM fuel cell stack is a sandwich-like structure composed of many layers, materials and interfaces. The pressure distribution in PEM fuel cell stack therefore is affected by the component material properties, geometrical parameters and the clamping method. In PEM fuel cells stack, all components are generally assembled between clamping plates by applying a torque moment on the tightening bolts; as a consequence the clamping force plays an important role for stack realization. The function of the stack-compression hardware is to fasten cell components with a defined and homogeneous pressure. If these requirements are not accurately fulfilled, the function and the durability of the cell will be influenced negatively. The MEAs and the bipolar plates need to be fixed in accurate positions and the compression of gaskets needs to be safe and homogeneous. If the pressure is too high, it will cause mechanical failure of the membrane or of the bipolar plate. Furthermore, an excessive compression of the components, in particular the GDL, increases the mass transport problems with a consequent reduction of cell performance and lifetime especially at high current density. If the pressure is too low, it may cause gas or cooling fluid leakage. Another effect of low compression is the increased contact resistance between the GDL and the bipolar plate, which will result in an inhomogeneous current distribution and thus in a reduced lifetime of the MEA.

Figure 5 shows the total displacement distribution with a maximum value near the edges in the PEM fuel cell stack during assembly process and also during operation for a number of cells equal to 1, 3 and 5. Bolts torque are equal for all simulations. The figures show the centre of the electrode tends to un-displacement. This un-displacement area increases by increasing the clamping torque. This effect confirms the hypothesis of plate deformation during the tightening. Furthermore, Figure 5 shows high deformations in the stack components during operation, about ten times higher than during assembly process. This is due to the more pressure producing from the thermal expansion of the stack components materials and membrane swelling during operation with a fixed relative position between the top and bottom end plates. These results are very clear in increasing of number of cells in the stack. During assembly process, the increasing in the number of cells increases the total displacement distribution. These status are different during operation, the increasing in the number of cells enhances the uniformity of the total displacement. Increasing the number of the cells leads to obtain more even contact pressure distribution.

Increasing the cell active area raises the cell power output, reduces the number of cells required to produce a given plant/system power output, and thus can reduce the cost of electricity, as long as the cell manufacturing yield and cell reliability are not adversely affected. Increasing the number of cells in a stack increases the voltage, while increasing the surface area of the cells increases the current.

In a stack of multiple cells, the compression differences between end cells and middle cells are unavoidable. The more uneven pressure distribution in middle cells can lead to reduced gas flows, which usually results in increased flooding. Increasing the number of cells enhances the uniformity of the mechanical state. The better contact pressure homogeneity is obtained with the greater number of cells and leads to the lower contact resistance. The Figures 6 - 16 show the stresses distribution in each component of the PEM fuel cell stack consisting of single cell during operation. While, the Figures 17 - 41 show the stresses distribution in each component of the PEM fuel cell stack consisting of three cells

during operation. In general, the results show lower stresses values with lower distributions and more homogeneous and uniformity in the stack that consisting of three cells.

The von Mises stress distribution of the cathode and anode end plates are shown in Figures 6 and 16 inside the single-cell stack and in Figures 17 and 41 inside the three-cell stack. In a conventional PEM fuel cell stack design, end plates are the two outermost components in a fuel cell assembly. They act as part of the clamping system to provide compressive force in order to unitize the single fuel cells together to form a stack. In addition, they also have some other important functions, such as ensuring good electrical contact between multiple layers within the fuel cell, ensuring good sealing at various interfaces, providing passages for the reactants, products and possibly cooling agents to enter and leave the fuel cell. Although the current design of fuel cell end plates can provide the above listed functions in a somewhat satisfactory manner, it is recognized that there are some existing problems to be solved, such as: deformation of end plates has an influence on fuel cell performance and is difficult to control; end plates are typically bulky and heavy, as compared to the fuel cell stacks; tie rods tend to loosen up during service. This may cause leakage, bad electrical contacts and deteriorated performance of the fuel cell stacks; and repeatability in pressure distribution can hardly be realized among the fuel cell stacks. The end plate material has a large influence on the mechanical properties of the end plate. A good end plate material has a high Young's modulus and a low density.

The von Mises stress distribution of the cathode and anode current plates are shown in Figures 7 and 15 inside the single-cell stack and in Figures 18 and 40 inside the three-cell stack. The current plate materials may influence fuel cell performance. Current plates for all kinds of fuel cell stacks are made of noble metals such as gold or platinum, or non-noble metals such as stainless steel, copper, or aluminum. The noble metals not only have good conductivity but also can almost avoid electrochemical corrosion and thus will not produce metallic ions that may poison the fuel cell. However, these noble metals are very expensive. If stainless steel, copper, or aluminum is directly used to make a current plate, electrochemical corrosion will occur if fluids pass through it, resulting in unwanted damage due to the metallic ions produced. In order to avoid this problem, nonnoble metal materials plated with gold or platinum are frequently used.

The von Mises stress distribution of the cathode and anode bipolar plates are shown in Figures 8 and 14 inside the single-cell stack and in Figures 19, 26, 33 and 25, 32, 39 inside the three-cell stack. Bipolar plates have traditionally been fabricated from high-density graphite on account of its superior corrosion resistance, chemical stability, high thermal conductivity, and availability. However, due to its molecular structure, it exhibits poor mechanical properties, high manufacturing cost, and it is difficult to work with. Nevertheless, graphite has established itself as the benchmark material for fabrication of bipolar plates, against which all other materials are compared. However, it is not suitable for either transportation applications that require good structural durability against shock and vibration or large-scale manufacturing because of its poor mechanical strength. The thickness of the graphite plates cannot be reduced, resulting in bulkiness and heaviness. As a result, recent studies have moved away from graphite in the direction of developing and optimizing more cost effective materials such as metals and composites.

Metallic materials are another choice for bipolar plates because of their good mechanical strength, high electrical conductivity, high thermal conductivity, high gas impermeability, low cost, and ease of manufacturing. The most advantage of metallic bipolar plates is stampability and reducing the thickness plate. Metallic bipolar plates can significantly reduce the volume of fuel cell stacks. In addition, relatively simple fabrication process of gas channels on the metallic plates by stamping enables mass production. In spite of these technical benefits, metallic plates are highly susceptible to corrosion which is closely related to reliability and durability of fuel cell engines. Recently, polymerecarbon composite bipolar plates have been investigated due to their lower cost, less weight, and higher corrosion resistivity in comparison with available materials such as graphite or metallic bipolar plates. The disadvantages of composite bipolar plates are non-stampability, lower electrical and mechanical properties than those of metallic bipolar plates.

In a fuel cell, gaskets are normally used to generate the insulation of anodic and cathodic compartments and to avoid gas cross over. Generally, they form a frame around MEA in the un-active zone of the flow field. The von Mises stress distribution of the cathode and anode gaskets are shown in Figures 9 and 13 inside the single-cell stack and in Figures 20, 27, 34 and 24, 31, 38 inside the three-cell stack. Because the cell plates are subject to a compression, the gasket material can influence the cell performance and durability. The use of different gasket materials changes the contact pressure distribution on the GDL,

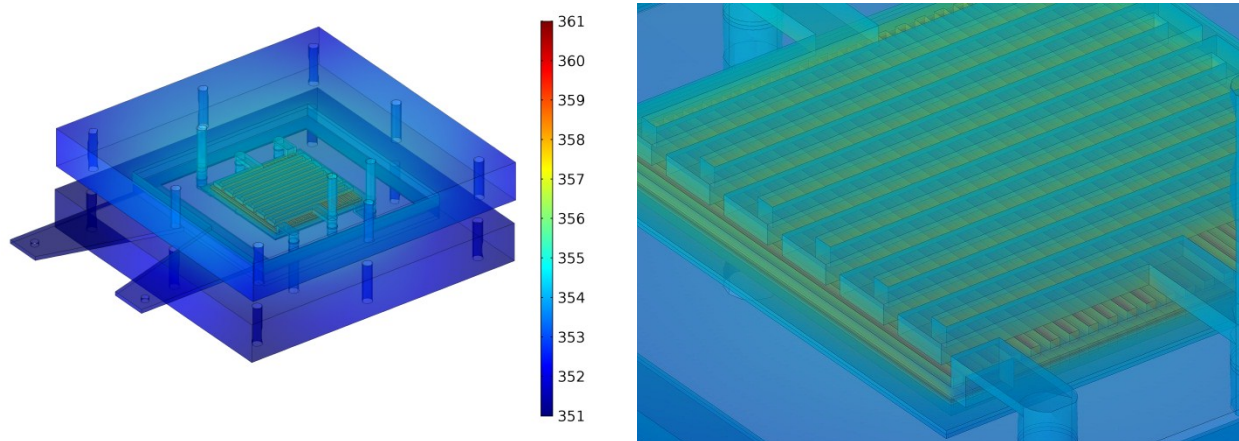
affecting the fuel cell performance and lifetime. Moreover, because of the gaskets are typically placed between the bipolar plates and the MEA to guarantee a good sealing, the chemical and mechanical characteristics and stability of the gasket materials must be investigated. In fact these properties are critical for both sealing and the electrochemical performance of the cell. Furthermore, it was found that there is an optimal difference in thickness between gaskets and GDL, in order to prevent problems related to an excessive GDL compression. Mismatch may lead to the following problems: (i) Thinner gasket may lead to sealing problem causing safety issue. In addition to that, the cell will be facing mass transport related losses. (ii) On the other hand, thicker gasket may result in poor contact between the bipolar plate and the GDL, which will be reflected on the ohmic region of the current voltage characteristics.

One of the key elements affecting PEM fuel cell stack performance is the GDL, which must provide a passage for reactant access and excess product removal to/from the catalyst layers, high electronic and thermal conductivity, and adequate mechanical support for the MEA. In order to fulfil these requirements, GDLs are typically made of highly porous carbon-fiber paper or cloth. The high porosity of these materials provides to the GDL a characteristic soft and flexible structure, susceptible of large deformations when subjected to compression. This leads to significant changes in its mechanical, electrical and thermal properties (thickness, porosity, permeability, electrical and thermal bulk conductivities and contact resistances, etc.), thus affecting mass, charge, and heat transfer processes, fuel cell performance and lifetime.

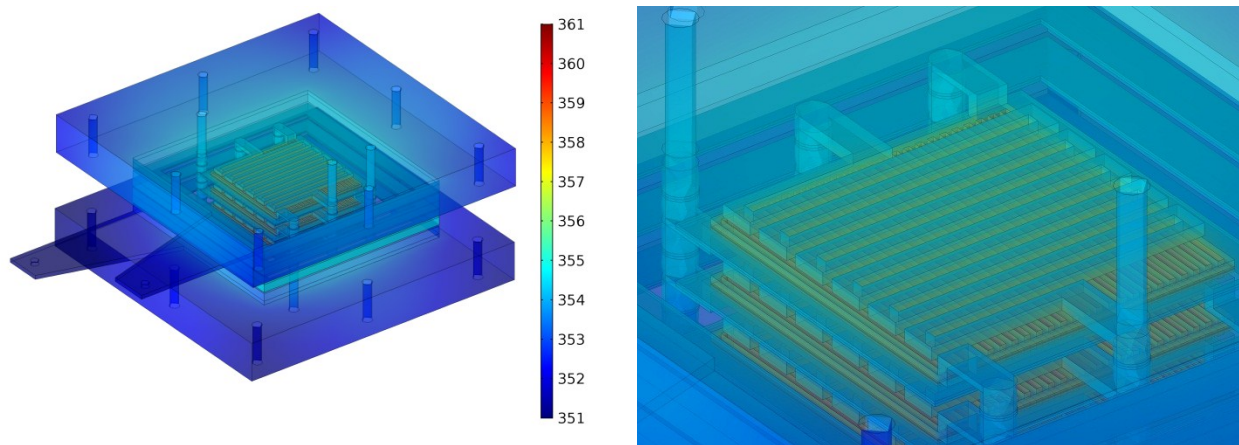
In the operation PEM fuel cell, the contact pressure on the GDL is increased because of the thermal expansion of cell materials and membrane swelling. Furthermore, due to the round corners of the bipolar plate, the contact behaviour at the interface is hard to predict without a CFD analysis. The von Mises stress distribution of the cathode and anode GDLs are shown in Figures 11 and 13 inside the single-cell stack and in Figures 22, 29, 36 and 24, 31, 38 inside the three-cell stack. The figures show that the GDL stress plot reveals good contact between the bipolar plate's channels and the carbon paper.

Each type of GDL material has its own optimal clamping pressure, to achieve a proper and uniform pressure distribution inside the stack. The inhomogeneous compression of the GDL leads to several opposing effects. On one hand, the assembly pressure improves both electric and thermal conductivities by reducing bulk and contact resistances. Slight compressions may also reduce mass transport resistance due to the shortening of the diffusion path to be covered by the reactants and products in their way to/from the catalyst layers. However, excessive compression loads may impede reactant and product transport due to the loss of pore volume, which is typically, accompanied by a reduction of the effective species diffusivities. On top of that, excessive assembly pressures are known to damage typical paper type GDLs, induce local delamination of the GDL under the channel, and result in non-uniform compressive loads which may degrade the membrane. Pore size reduction may also affect multiphase capillary transport phenomena in the GDL (liquid water removal in PEM fuel cells). And last, but not least, partial GDL intrusion into the channel produces a reactant flow rate reduction or, alternatively, an increase of the parasitic power required to maintain the flow, which affects the overall efficiency of the stack.

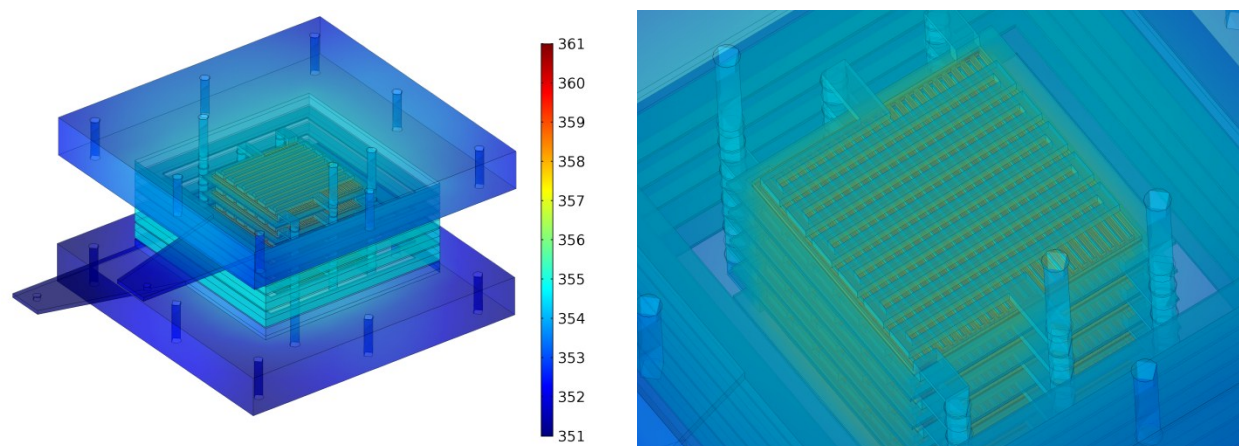
The heart of a fuel cell is a polymer, proton exchange membrane (PEM). On both sides of the membrane there are catalyst layer. Mechanical stresses which limit MEA durability have two origins. Firstly, this is the stresses arising during fuel cell assembly (bolt assembling). The bolts provide the tightness and the electrical conductivity between the contact elements. Secondly, additional mechanical stresses occur during fuel cell running because PEM fuel cell components have different thermal expansion and swelling coefficients. Thermal and humidity gradients in the fuel cell produce dilatations obstructed by tightening of the screw-bolts. Compressive stress increasing with the hygro-thermal loading can exceed the yield strength which causes the plastic deformation. The mechanical behaviour of the membrane depends strongly on clamping pressure, hydration and temperature. Furthermore, in an operating fuel cell, because the four sides of the membranes are fixed, variations in temperature and humidity during operation can induce MEA dimensional change and corresponding cyclic stresses and strains inside it. Mechanical MEA degradation can occur in many forms, such as MEA thinning, tears, cracks, pinholes, and so on. The von Mises stress distributions of the MEAs are shown in Figure 11 inside the single-cell stack and in Figures 22, 29, 36 inside the three-cell stack. The figures show that the stresses distribution over the active area of fuel cell stack with single-cell is more uneven than the three-cell.



(a) PEM fuel cell stack consisting of single cell.

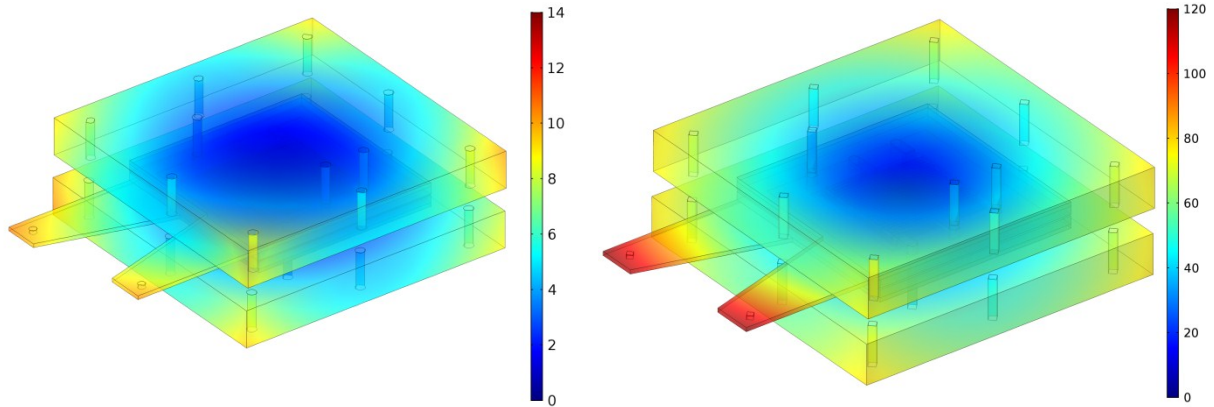


(b) PEM fuel cell stack consisting of three cells.



(c) PEM fuel cell stack consisting of five cells.

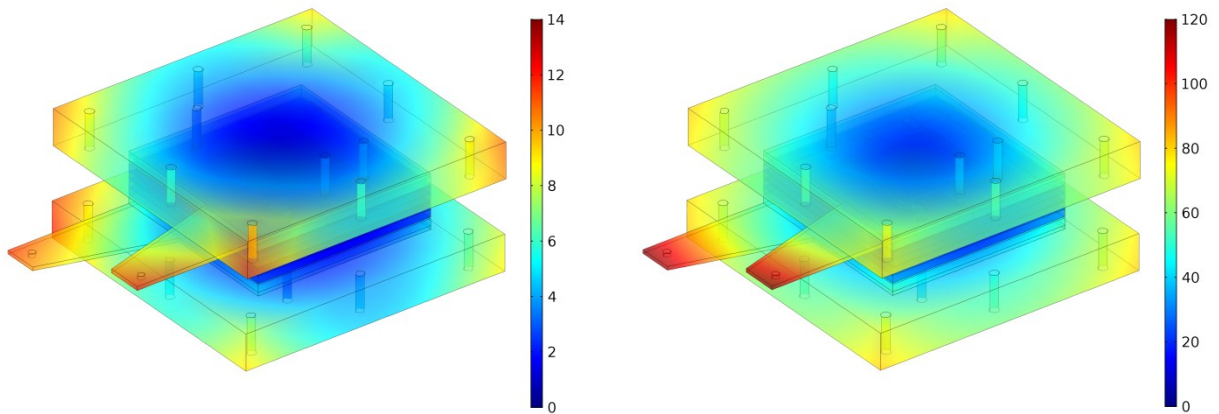
Figure 4. Solid-phase temperature distribution in the PEM fuel cell stack during operation [K].



During assembly process.

During operation.

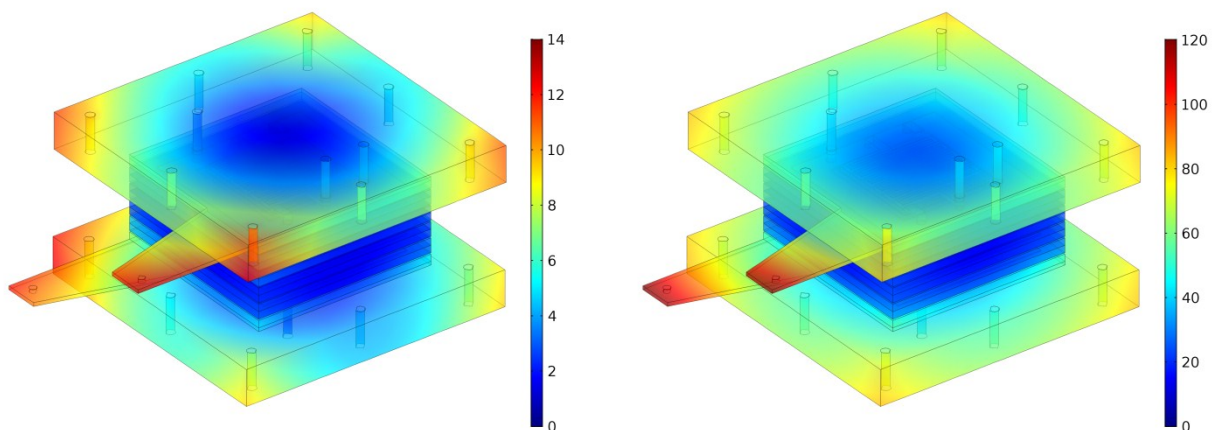
(a) PEM fuel cell stack consisting of single cell.



During assembly process.

During operation.

(b) PEM fuel cell stack consisting of three cells.



During assembly process.

During operation.

(c) PEM fuel cell stack consisting of five cells.

Figure 5. Total displacement distribution in the PEM fuel cell stack [μm].

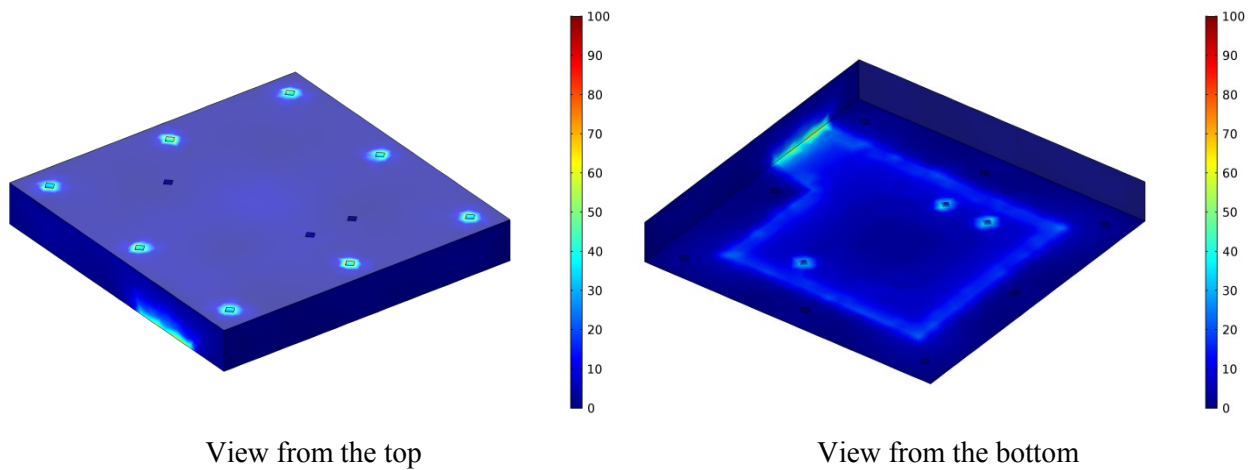


Figure 6. Cathode end plate von Mises stress distribution in the single-cell stack during operation [MPa].

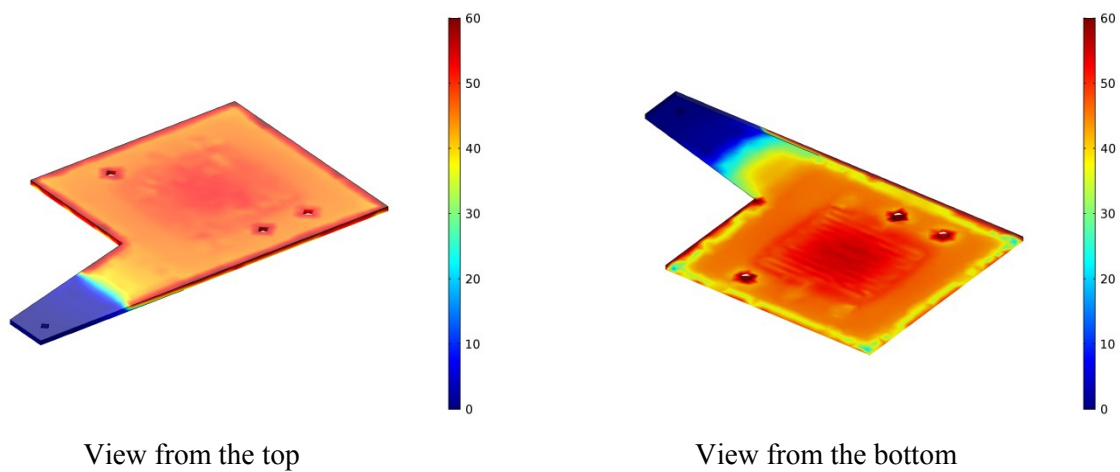


Figure 7. Cathode current plate von Mises stress distribution in the single-cell stack during operation [MPa].

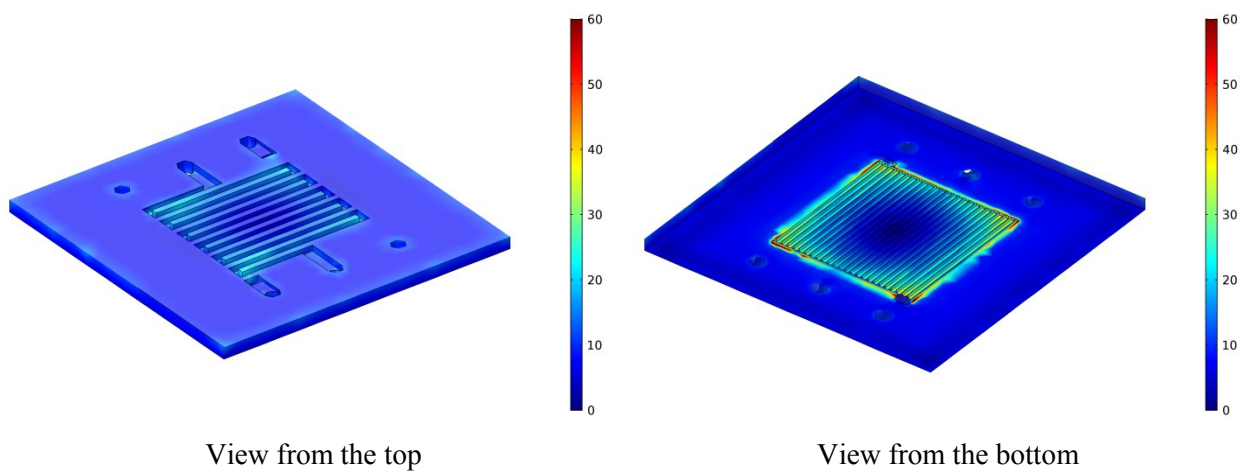


Figure 8. Cathode bipolar plate von Mises stress distribution in the single-cell stack during operation [MPa].

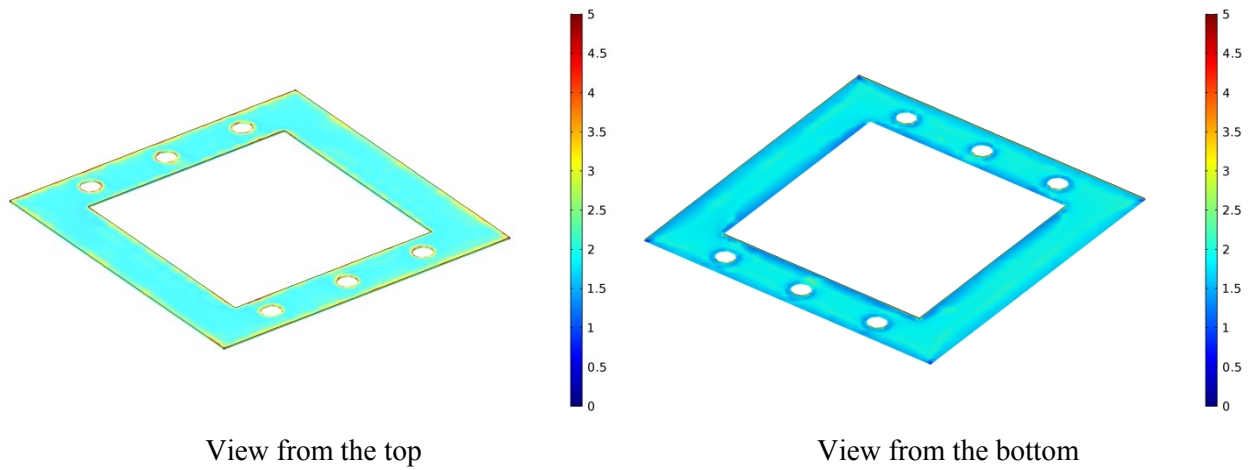


Figure 9. Cathode gasket von Mises stress distribution in the single-cell stack during operation [MPa].

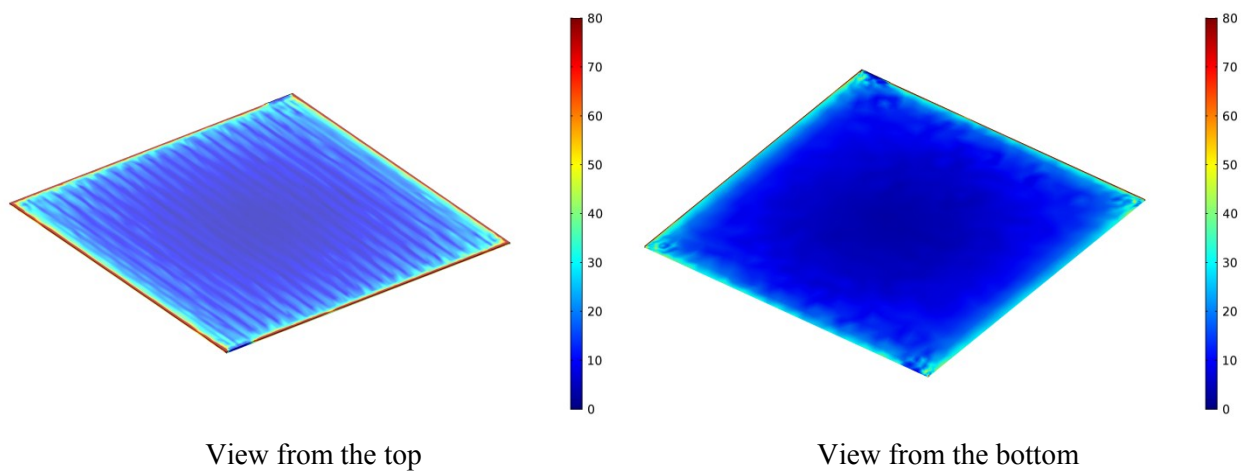


Figure 10. Cathode GDL von Mises stress distribution in the single-cell stack during operation [MPa].

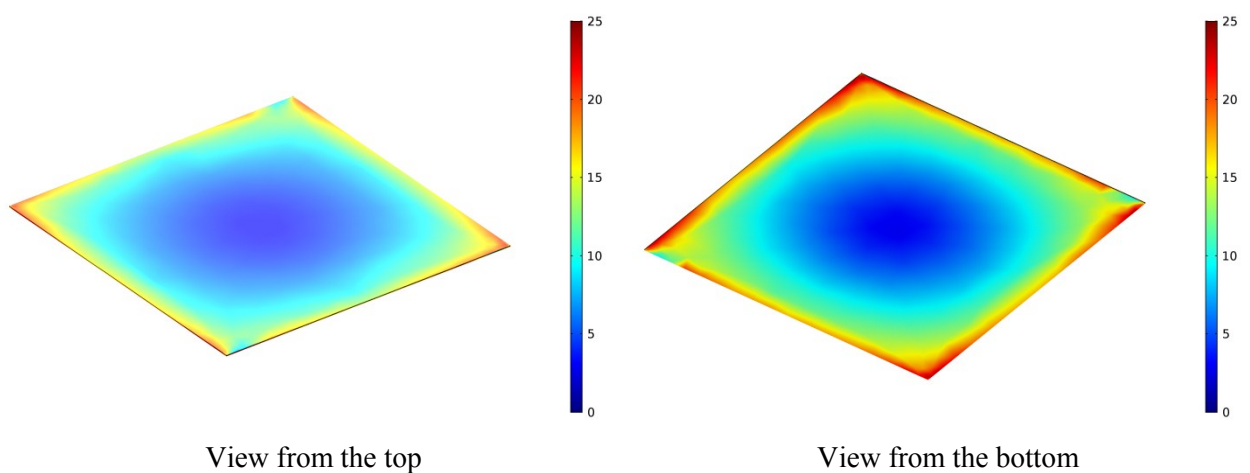


Figure 11. MEA von Mises stress distribution in the single-cell stack during operation [MPa].

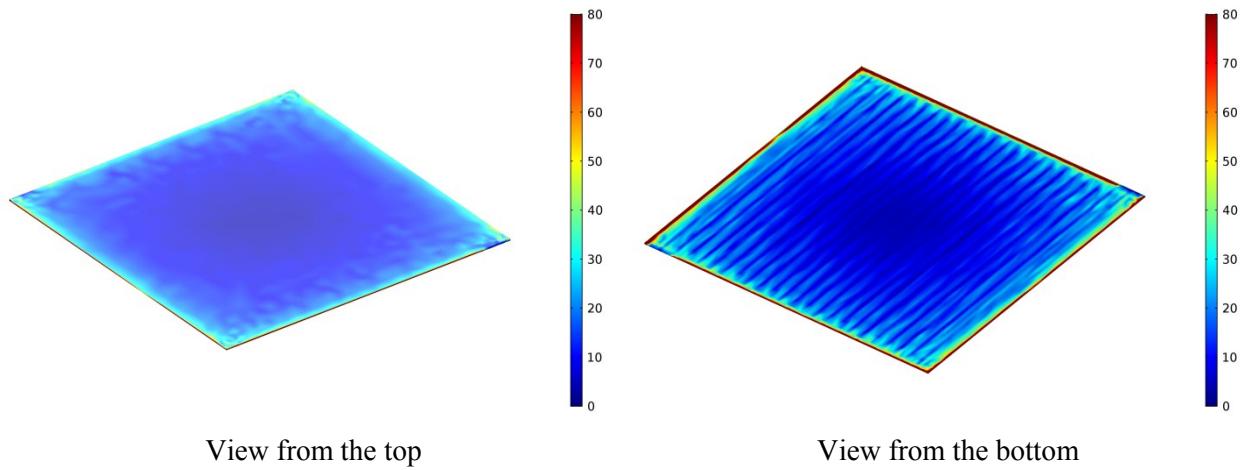


Figure 12. Anode GDL von Mises stress distribution in the single-cell stack during operation [MPa].

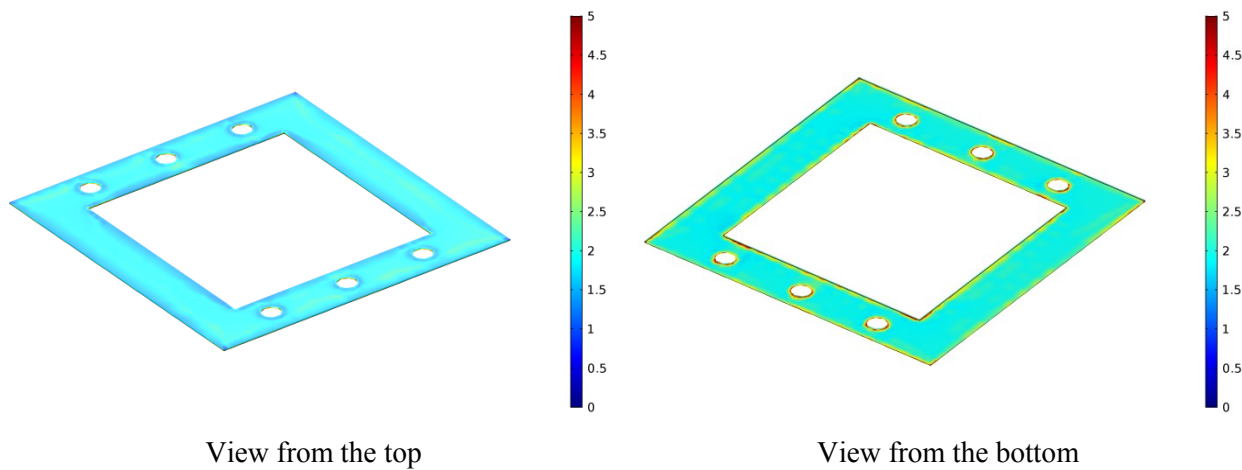


Figure 13. Anode gasket von Mises stress distribution in the single-cell stack during operation [MPa].

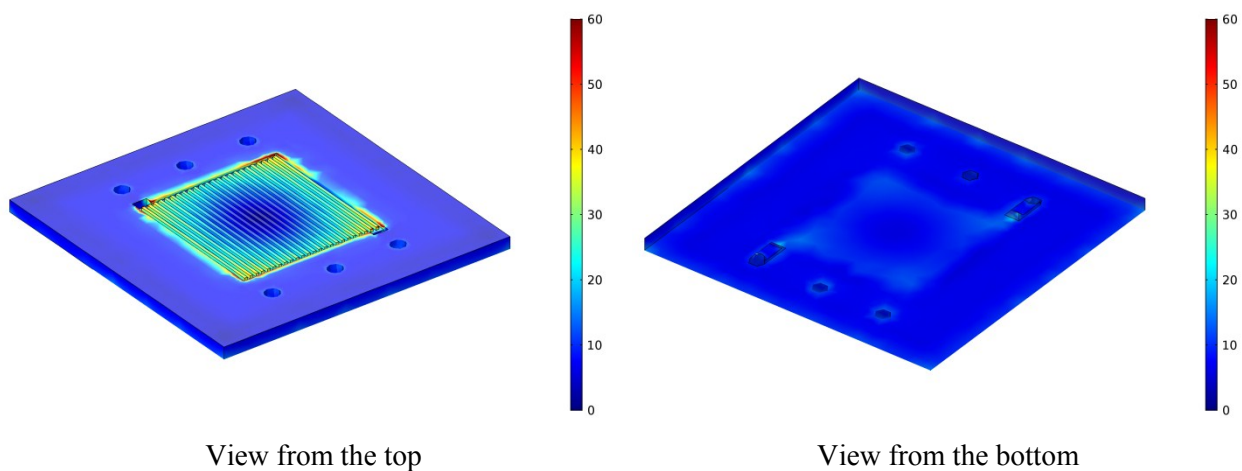


Figure 14. Anode bipolar plate von Mises stress distribution in the single-cell stack during operation [MPa].

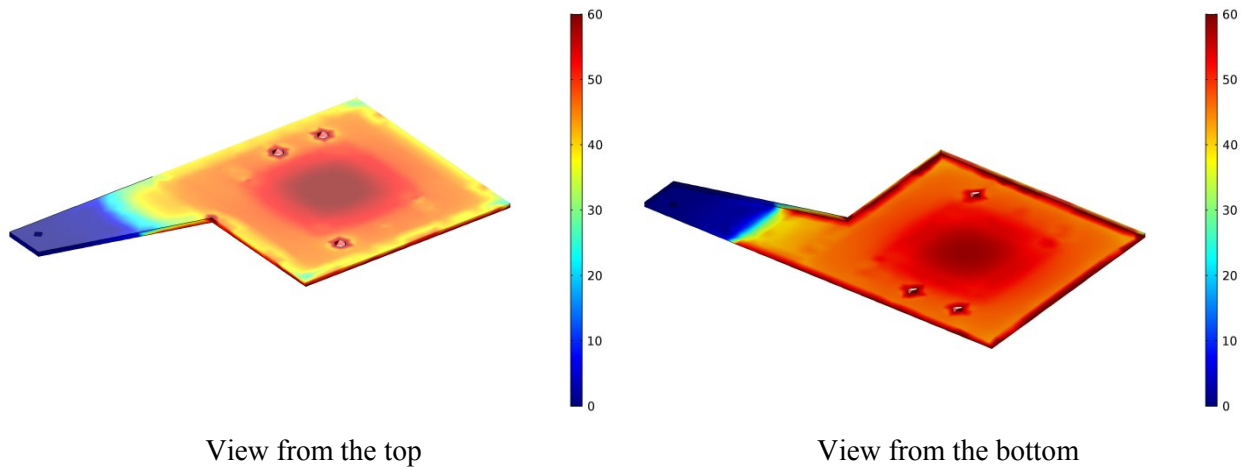


Figure 15. Anode current plate von Mises stress distribution in the single-cell stack during operation [MPa].

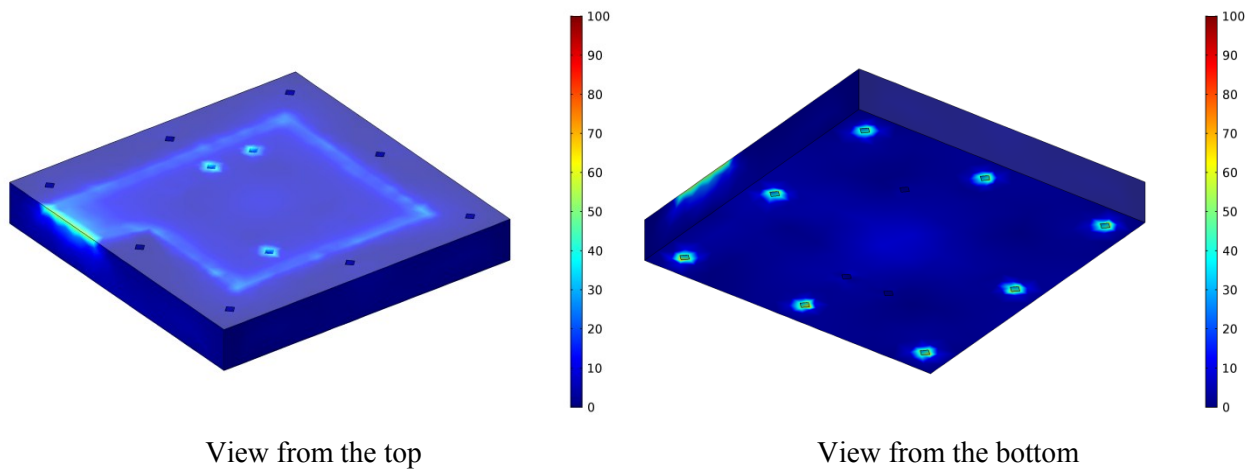


Figure 16. Anode end plate von Mises stress distribution in the single-cell stack during operation [MPa].

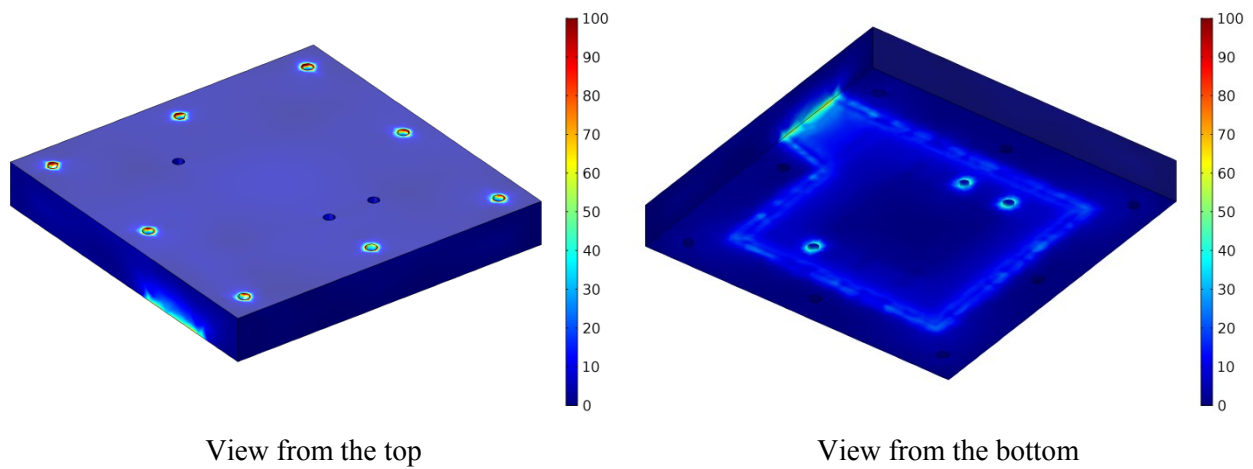


Figure 17. Cathode end plate von Mises stress distribution in the three-cell stack during operation [MPa].

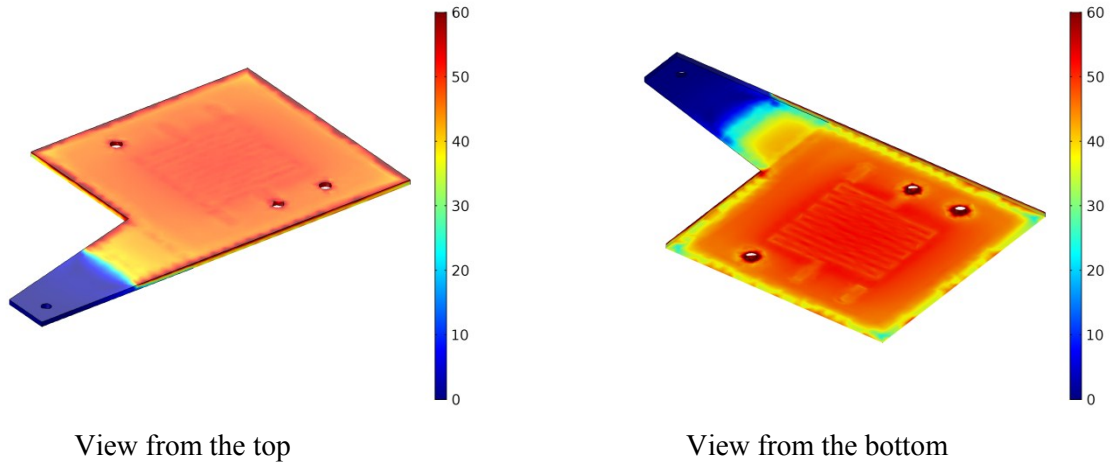


Figure 18. Cathode current plate von Mises stress distribution in the three-cell stack during operation [MPa].

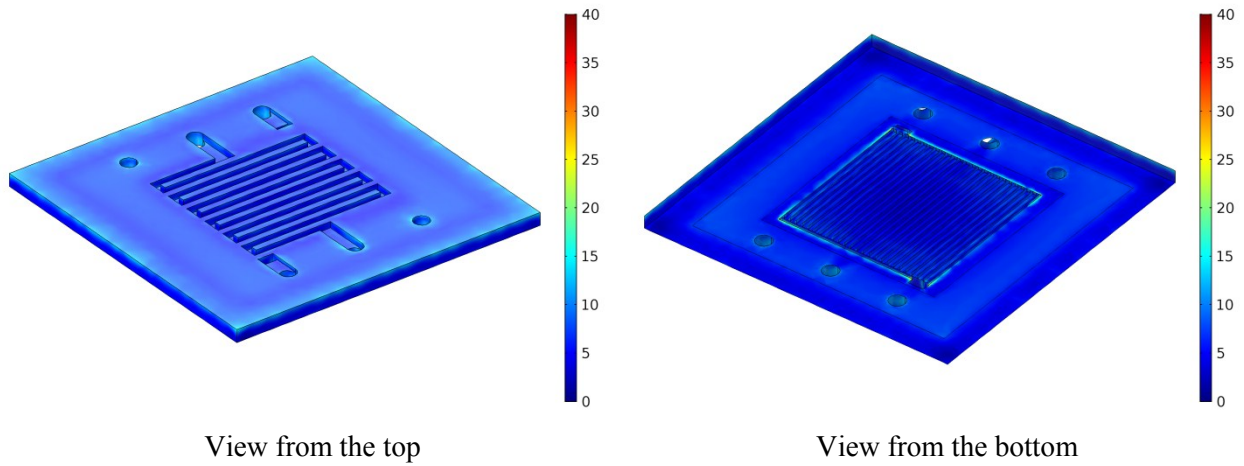


Figure 19. 1st cell cathode bipolar plate von Mises stress distribution in the three-cell stack during operation [MPa].

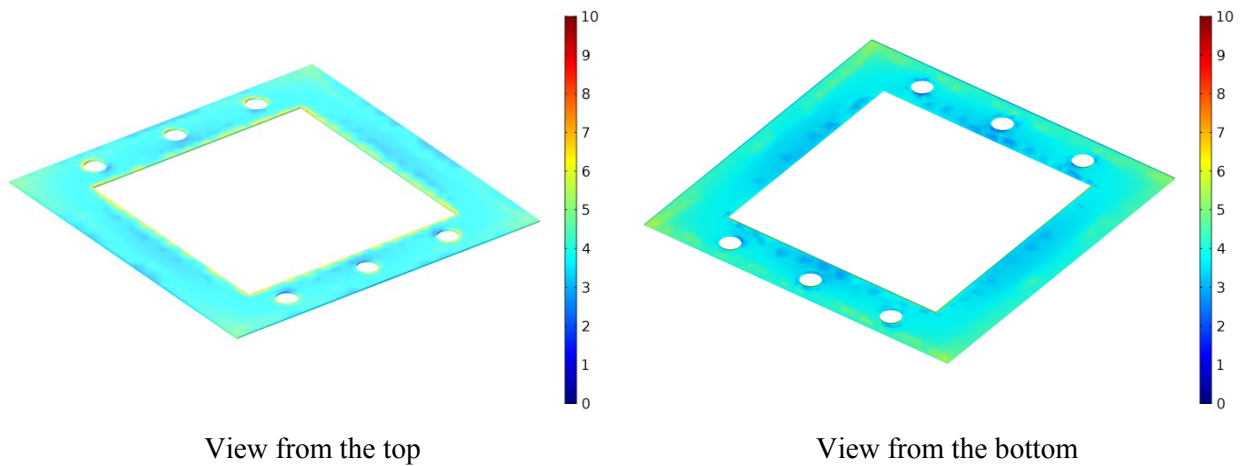


Figure 20. 1st cell cathode gasket von Mises stress distribution in the three-cell stack during operation [MPa].

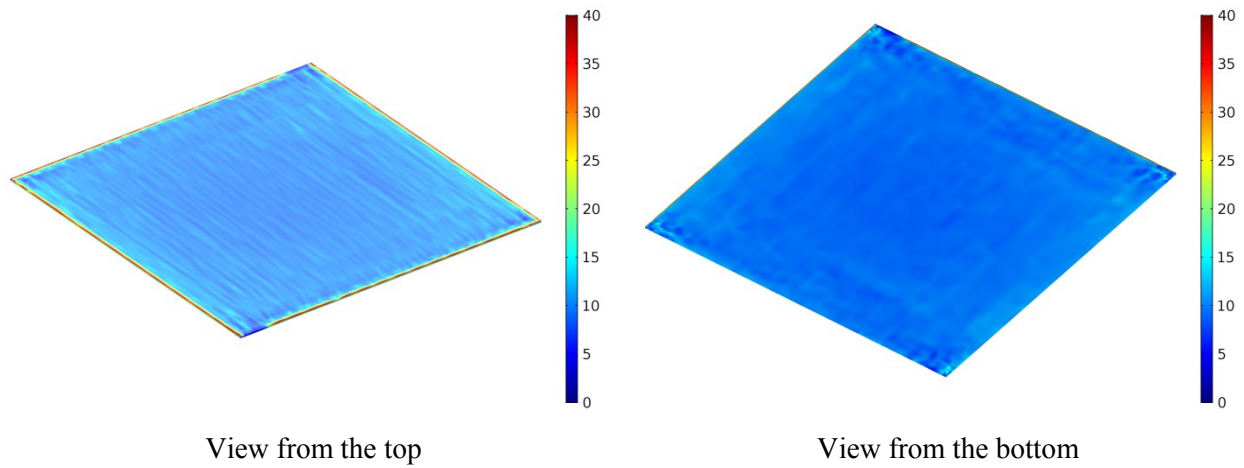


Figure 21. 1st cell cathode GDL von Mises stress distribution in the three-cell stack during operation [MPa].

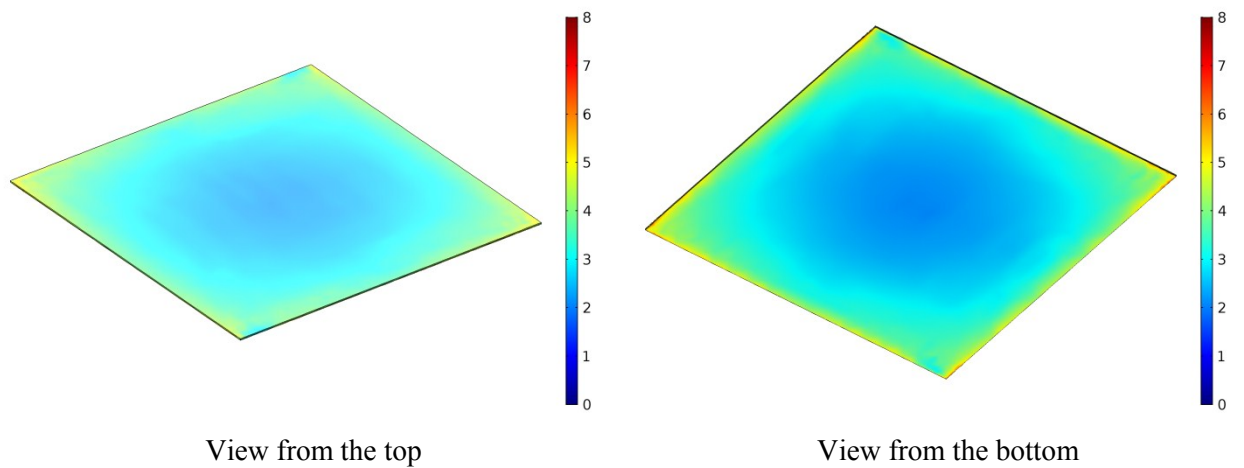


Figure 22. 1st cell MEA von Mises stress distribution in the three-cell stack during operation [MPa].

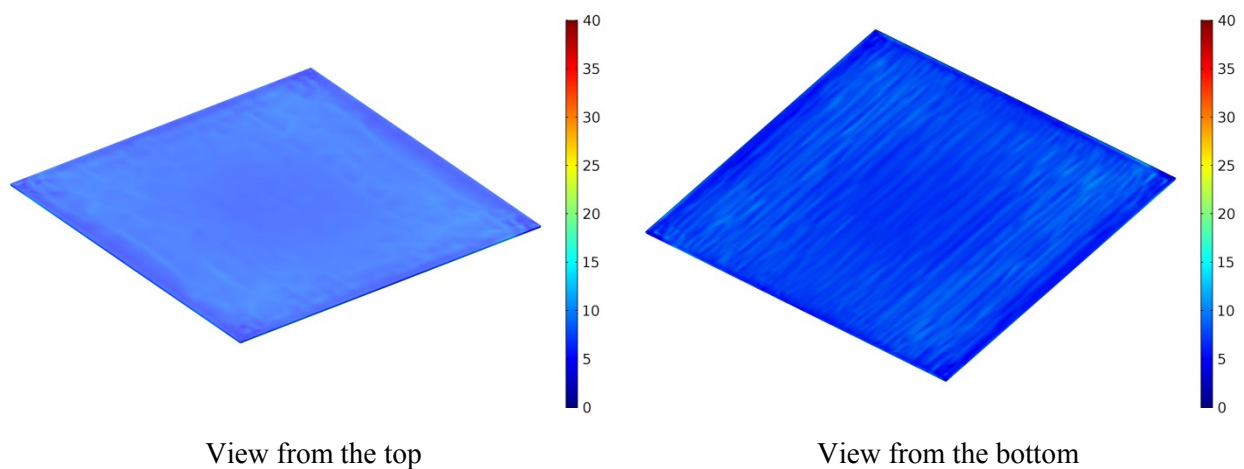


Figure 23. 1st cell anode GDL von Mises stress distribution in the three-cell stack during operation [MPa].

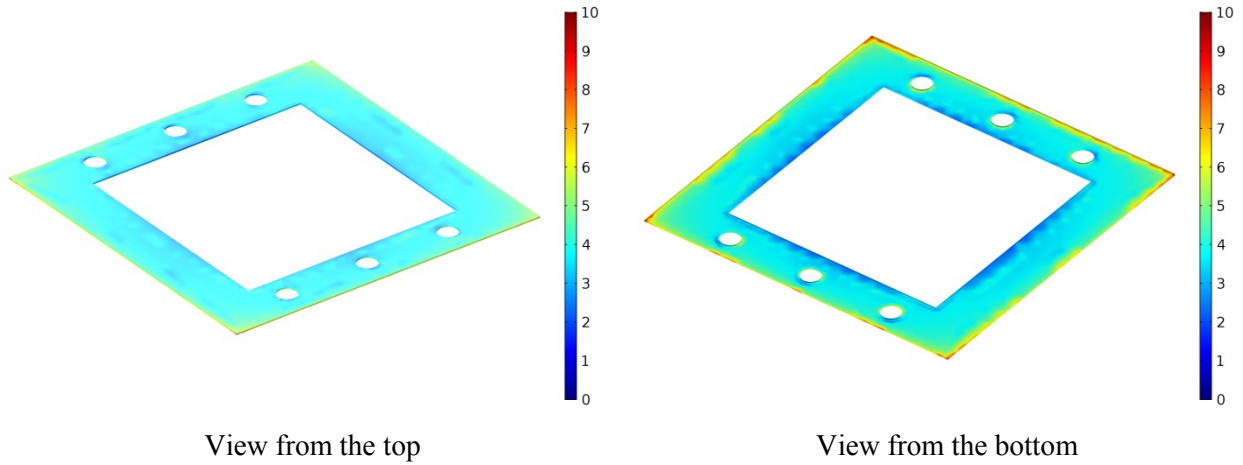


Figure 24. 1st cell anode gasket von Mises stress distribution in the three-cell stack during operation [MPa].

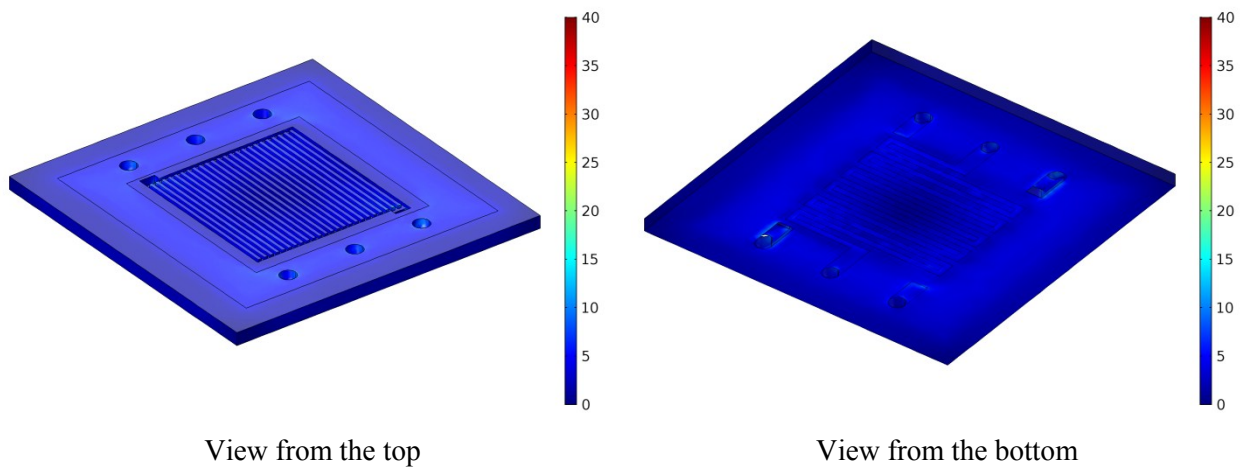


Figure 25. 1st cell anode bipolar plate von Mises stress distribution in the three-cell stack during operation [MPa].

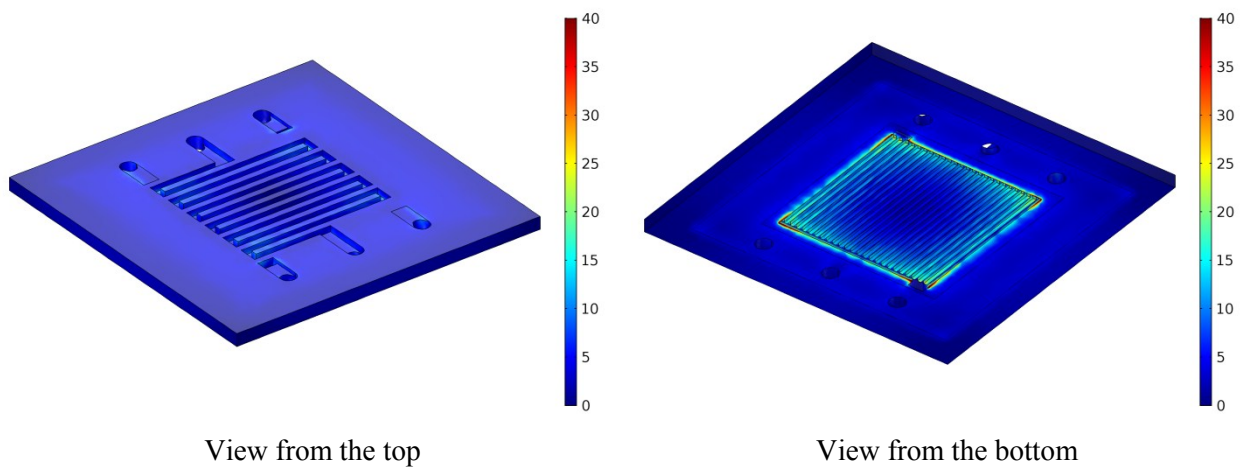


Figure 26. 2nd cell cathode bipolar plate von Mises stress distribution in the three-cell stack during operation [MPa].

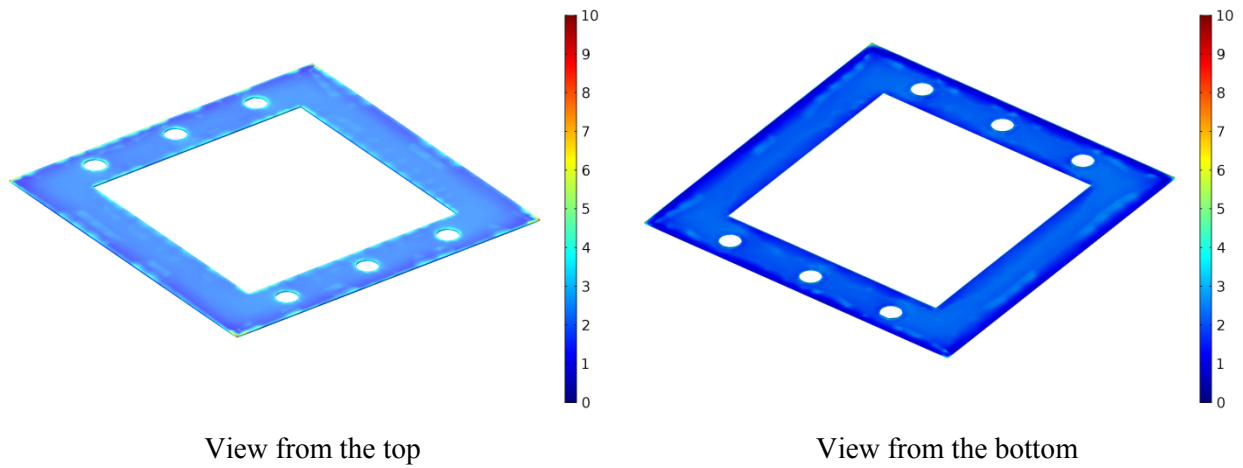


Figure 27. 2nd cell cathode gasket von Mises stress distribution in the three-cell stack during operation [MPa].

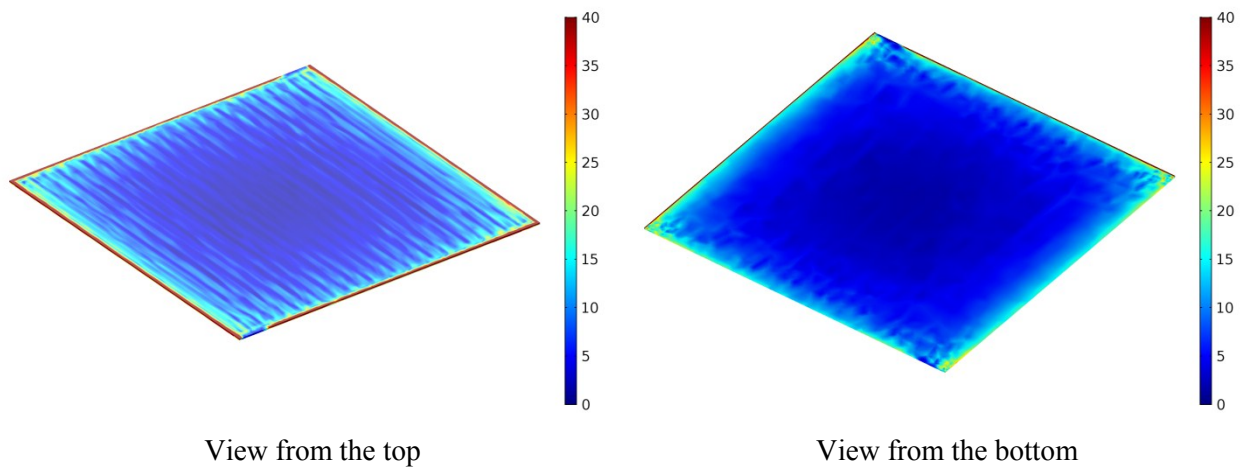


Figure 28. 2nd cell cathode GDL von Mises stress distribution in the three-cell stack during operation [MPa].

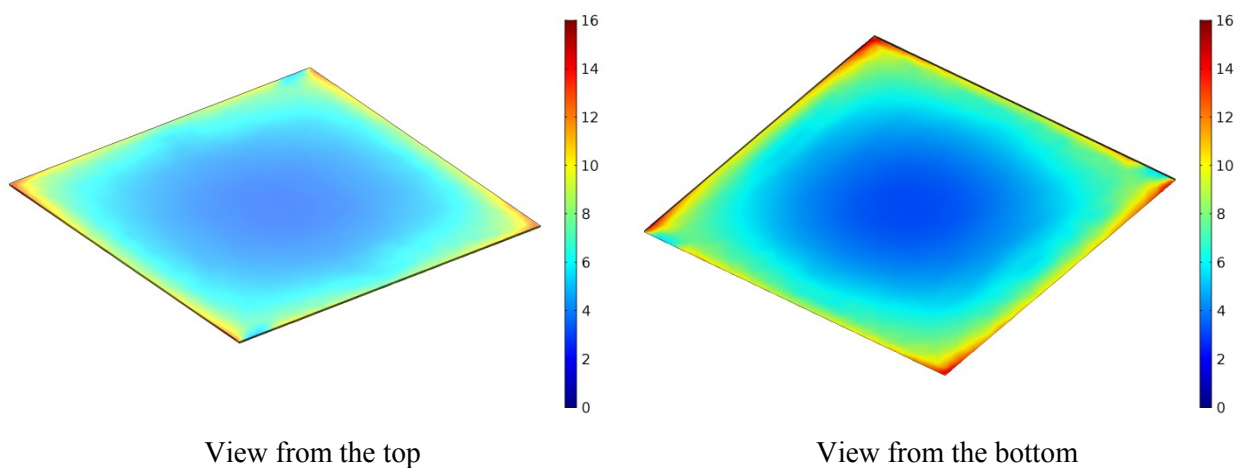


Figure 29. 2nd cell MEA von Mises stress distribution in the three-cell stack during operation [MPa].

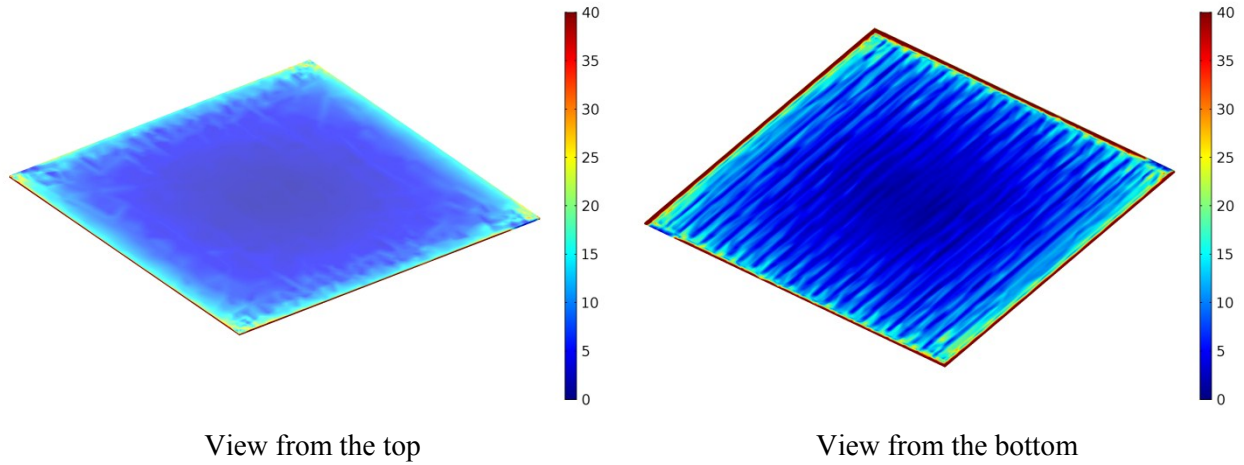


Figure 30. 2nd cell anode GDL von Mises stress distribution in the three-cell stack during operation [MPa].

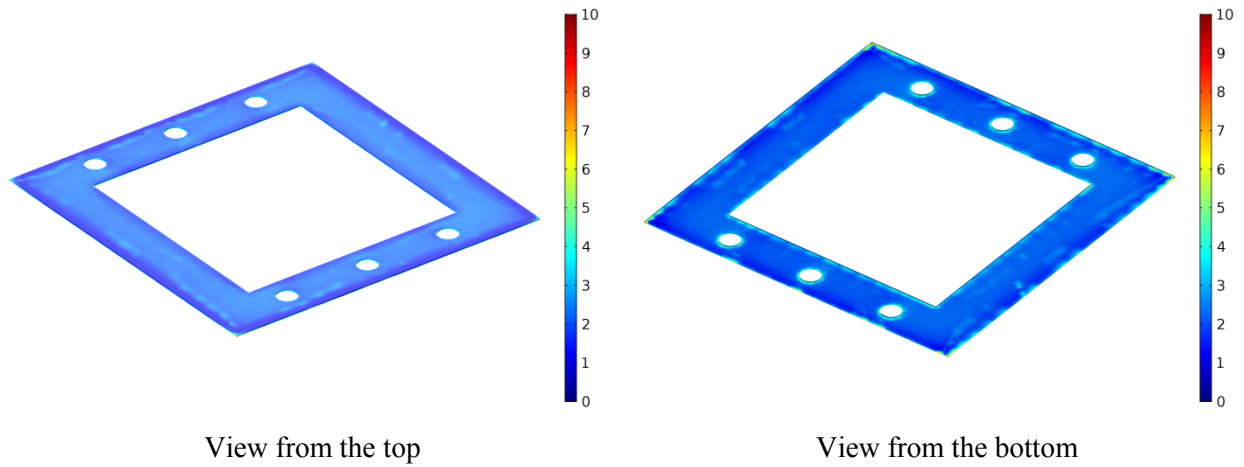


Figure 31. 2nd cell anode gasket von Mises stress distribution in the three-cell stack during operation [MPa].

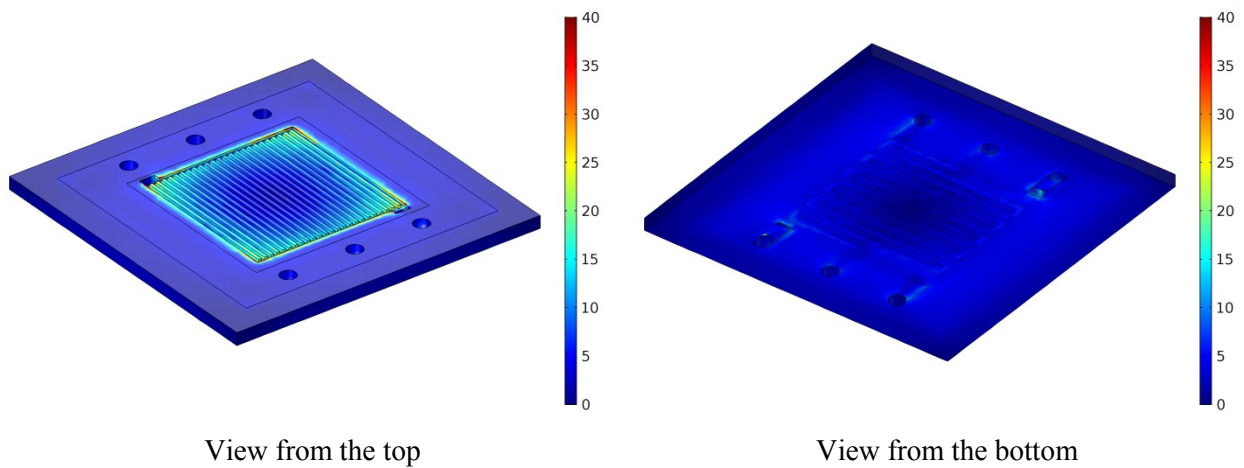


Figure 32. 2nd cell anode bipolar plate von Mises stress distribution in the three-cell stack during operation [MPa].

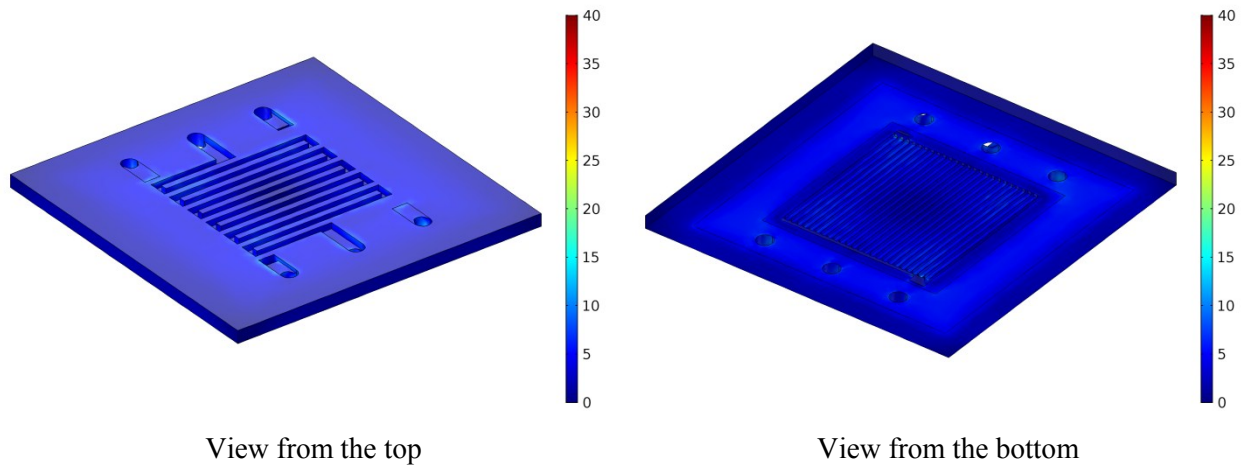


Figure 33. 3rd cell cathode bipolar plate von Mises stress distribution in the three-cell stack during operation [MPa].

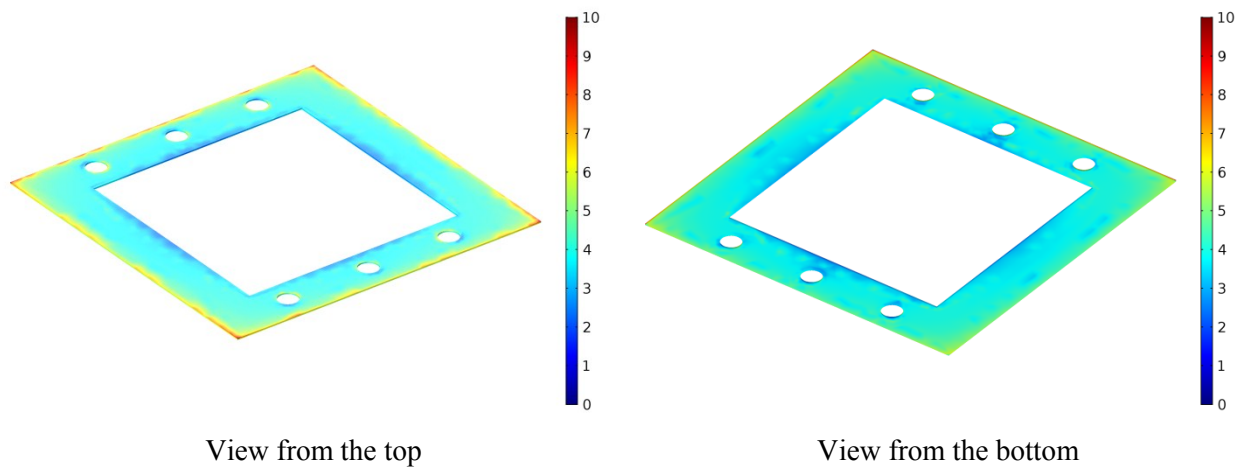


Figure 34. 3rd cell cathode gasket von Mises stress distribution in the three-cell stack during operation [MPa].

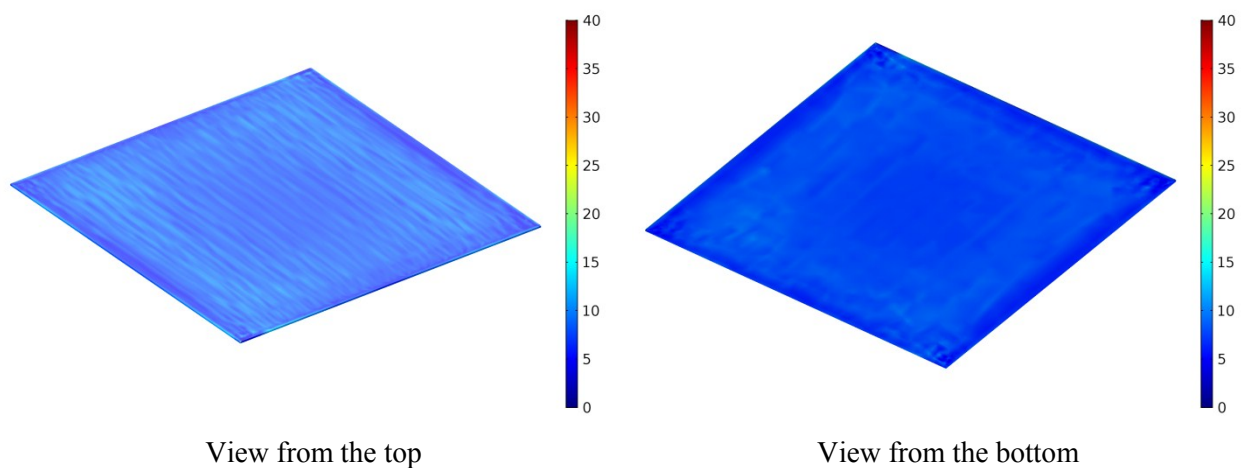


Figure 35. 3rd cell cathode GDL von Mises stress distribution in the three-cell stack during operation [MPa].

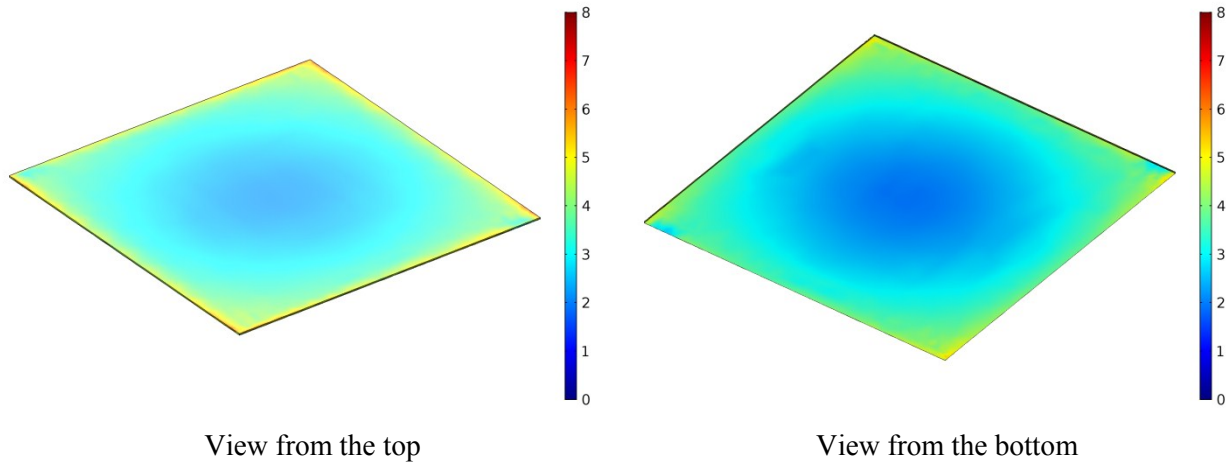


Figure 36. 3rd cell MEA von Mises stress distribution in the three-cell stack during operation [MPa].

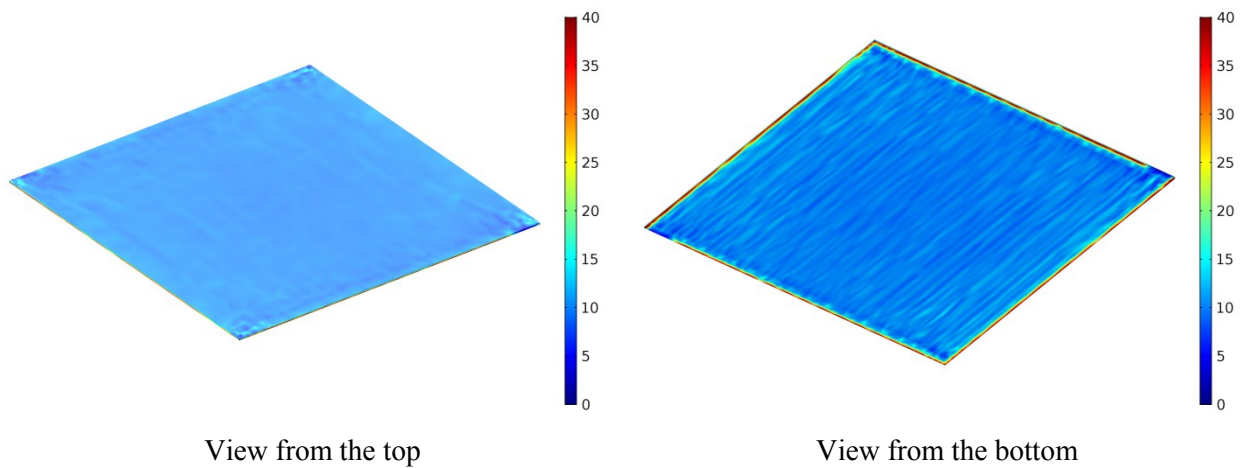


Figure 37. 3rd cell anode GDL von Mises stress distribution in the three-cell stack during operation [MPa].

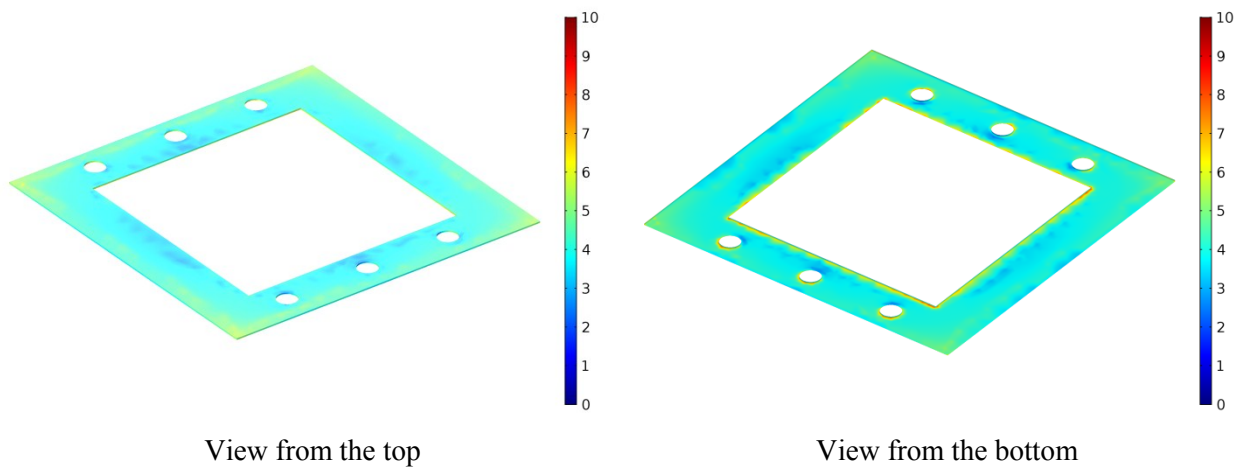


Figure 38. 3rd cell anode gasket von Mises stress distribution in the three-cell stack during operation [MPa].

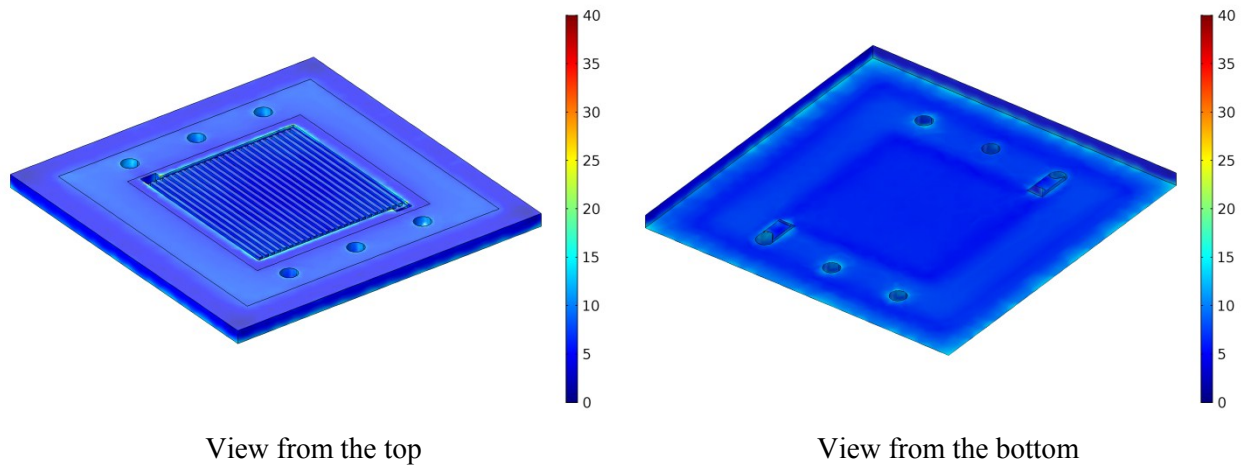


Figure 39. 3rd cell anode bipolar plate von Mises stress distribution in the three-cell stack during operation [MPa].

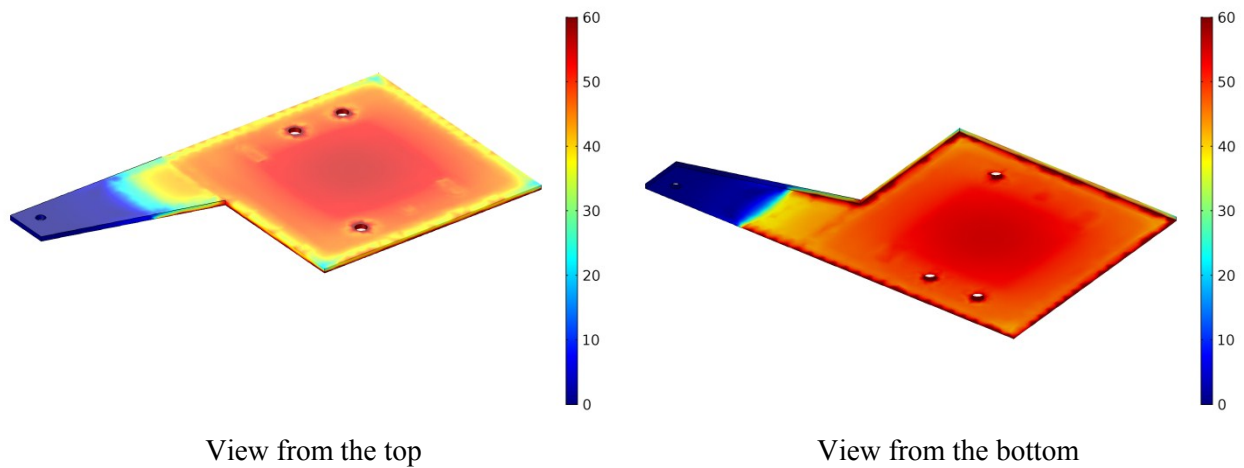


Figure 40. Anode current plate von Mises stress distribution in the three-cell stack during operation [MPa].

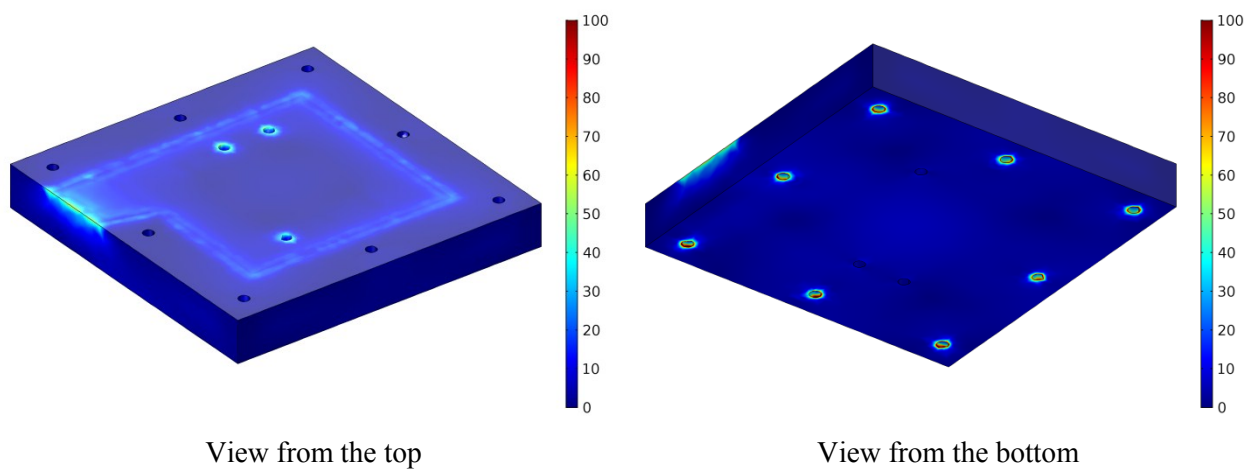


Figure 41. Anode end plate von Mises stress distribution in the three-cell stack during operation [MPa].

4. Conclusion

Durability of PEM fuel cell stack components remains, in most cases, insufficiently understood. Lengthy required testing times and the difficulty of performing in-situ, non-destructive structural evaluation of key components makes the topic a difficult one. Investigating the mechanical response of the PEM fuel cell stack during operation requires studying and modeling of the stress-strain behavior of all fuel cell stack components in operation phase. Three dimensional non-isothermal solid mechanics-CFD model of a PEM fuel cell stack, integrating the real full scale geometry of all components have been used to study the influence of the number of cells on the stress distribution in a running PEM fuel cell stack. Simulation of a running multi cells stack was successful and has not been previously seen in literatures work. The results showed that the center of the electrode tends to un-displacement. This un-displacement area increases by increasing the clamping torque. The deformations in the stack components during operation were about ten times higher than during assembly process. During assembly process, the increasing in the number of cells increases the total displacement distribution. These status were different during operation, the increasing in the number of cells enhances the uniformity of the total displacement. Increasing the number of cells enhances the uniformity of the mechanical state. The better contact pressure homogeneity was obtained with the greater number of cells and leads to the lower contact resistance. In general, the results showed lower stresses values with lower distributions and more homogeneous and uniformity in the stack that consisting of multi cells.

Acknowledgements

This work was supported by International Energy and Environment Foundation (IEEF).

References

- [1] Maher A.R. Sadiq Al-Baghdadi. PEM Fuel Cells-from Single Cell to Stack: Fundamentals, Modeling, Analysis, and Applications. International Energy and Environment Foundation, 2015.
- [2] Maher A.R. Sadiq Al-Baghdadi. Proton exchange membrane fuel cells modeling: A review of the last ten years results of the Fuel Cell Research Center-IEEF. International Journal of Energy and Environment 2017, 8(1); pp.1-28.
- [3] Maher A.R. Sadiq Al-Baghdadi. Modeling optimizes PEM fuel cell durability using three-dimensional multi-phase computational fluid dynamics model. International Journal of Energy and Environment. 2010, 1(3); pp. 375-398.
- [4] Maher A.R. Sadiq Al-Baghdadi. Prediction of deformation and hygro-thermal stresses distribution in PEM fuel cell vehicle using three dimensional CFD model. International Journal of Energy and Environment IJEE, 2012; 3(4), 485-504.
- [5] Maher A.R. Sadiq Al-Baghdadi. A CFD study of hygro-thermal stresses distribution in PEM fuel cell during regular cell operation. Renewable Energy 2009, 34(3); pp.674-682.
- [6] Wen C-Y, Lin Y-S, Lu C-H. Experimental study of clamping effects on the performances of a single proton exchange membrane fuel cell and a 10-cell stack. Journal of Power Sources 2009; 192, pp.475-485.
- [7] Christophe Carral, Patrice Mele. A numerical analysis of PEMFC stack assembly through a 3D finite element model. Int. J. Hydrogen Energy 2014; 39, pp.4516-4530.
- [8] Alex Bates, Santanu Mukherjee, Sunwook Hwang, Sang C. Lee, Osung Kwon, Gyeong Ho Choi, Sam Park. Simulation and experimental analysis of the clamping pressure distribution in a PEM fuel cell stack. Int. J. Hydrogen Energy 2013; 38, pp.6481-6493.
- [9] Javier de la Cruz, Ulises Cano, Tatiana Romero. Simulation and in situ measurement of stress distribution in a polymer electrolyte membrane fuel cell stack. Journal of Power Sources 2016; 329, pp.273-280.
- [10] Willy Charon, Marie-Christine Itchev, Jean-Francois Blachot. Mechanical simulation of a Proton Exchange Membrane Fuel Cell stack using representative elementary volumes of stamped metallic bipolar plates. Int. J. Hydrogen Energy 2014; 39, pp.13195-13205.
- [11] Chi-Hui Chien, Yao-Lun Hu, Ting-Hsuan Su, Hsuan-Ting Liu, Chung-Ting Wang, Ping-Feng Yang, Ying-Xu Lu. Effects of bolt pre-loading variations on performance of GDL in a bolted PEMFC by 3-D FEM analysis. Energy 2016; 113, pp.1174-1187.
- [12] Maher A.R. Sadiq Al-Baghdadi. Three-dimensional solid mechanics-CFD modeling of a PEM fuel cell stack. International Journal of Energy and Environment 2018, 9(1); pp.1-26.